nature REVIEWS

Nature Reviews referee guidelines

Review articles

Nature Reviews publishes timely, authoritative articles that are of broad interest and exceptional quality. Thank you for taking the time to help us to ensure that our articles meet these high standards.

Review articles in *Nature Reviews* journals provide accessible, authoritative and balanced overviews of a field or topic. These articles are targeted towards readers from advanced undergraduate level and upwards, including researchers, academics and clinicians, and should be accessible to readers working in any discipline.

Please submit your report in narrative form and provide detailed justifications for all statements. Confidential comments to the editor are welcome, but it is helpful if the main points are stated in the comments for transmission to the authors.

Please note that all *Nature Reviews* articles will be thoroughly edited before publication and all figures will be redrawn by our in-house art editors. We therefore request that you concentrate on the scientific content of the article, rather than any minor errors in language or grammar.

Please consider and comment on the following points when reviewing this manuscript:

- Is the article timely and does it provide a useful addition to the existing literature?
- Are the scope and aims of the article clear?
- Are the ideas logically presented and discussed?
- Is the article accessible to a wide audience, including readers who are not specialists in your own field?
- Does the article provide a balanced overview of the literature? Please bear in mind that it may not be possible to cover all aspects of a field within such a concise article.
- Does the article provide new insight into recent advances?
- Is the discussion fair and accurate? Although our authors are encouraged to be opinionated, they should not ignore alternative points of view.
- Do the figures, boxes and tables provide clear and accurate information? Are there any additional or alternative display items that you think that the authors should include?
- Are the references appropriate and up-to-date? Do they reflect the scope of the article?
- Are you aware of any undeclared conflicts of interest that might affect the balance, or perceived balance, of the article?

Time-Resolved Transmission Electron Microscopy for Nanoscale Chemical Dynamics

Francis M. Alcorn[¶], Prashant K. Jain[¶*], Renske M. van der Veen[¶§*]

[¶]*Department of Chemistry and Materials Research Laboratory, University of Illinois Urbana-Champaign, Urbana, IL, USA*

[§]*Department Atomic-Scale Dynamics in Light-Energy Conversion, Photon Science Division, Helmholtz Center Berlin for Materials and Energy, Germany*

[*]*renske.vanderveen@helmholtz-berlin.de*

[*]*jain@illinois.edu*

Abstract

Transmission electron microscopy (TEM) had its genesis in the physics and biology communities, but it has become an indispensable addition to the modern-day chemist's toolkit. Due to its capability of imaging structure on length scales ranging from millimeters to angstroms, TEM has enabled unprecedented understanding of the atomic structures of materials and the relationships between atomic structure, properties, and function. Recent developments in TEM technologies have advanced the technique beyond static material characterization to the real-time probing of structural evolution on the nanoscale. The range of available, chemically relevant stimuli is vast—including heating, light illumination, gas/liquid exposure, electrical bias, and even mechanical perturbations—and continues to grow. Accompanying advances in data collection technologies have pushed the temporal resolution into the microsecond (10^{-6} s) regime with the use of direct-electron detectors and down to the femtosecond (10^{-15} s) regime with pump–probe microscopy. Consequently, studies have deftly applied TEM for understanding of nanoscale dynamics, often *in operando*. Herein, time-resolved *in situ* TEM techniques and their applications for probing several classes of chemical and physical processes are discussed, along with emerging directions in the TEM field.

Introduction

Materials invariably undergo structural rearrangements over the course of their functioning within a device. Such restructuring of a material may enhance or activate desired properties, or they may underlie losses in performance and degradation of the device. Notable examples from catalysis include the activation of alloyed gold-based nanoparticles exposed to reactant gases[1] or the degradation of copper catalysts by the formation of nanoclusters during electrochemical CO_2 reduction[2]. Static *pre-* and *post-mortem* characterization of a material that has been subjected to a change in environment offers a limited view of the relationship between structure, property, and function. What is missing in such characterization is a real-time look at how atoms rearrange over the course of a chemical transformation. This knowledge is crucial for the rational bottom-up design and optimization of functional materials and facilitating the translation of basic science to technological applications. Hence, a large body of recent research has focused on developing and applying appropriate tools to follow the ensuing atomic-scale materials dynamics under realistic, ideally operating conditions of a device. Among these tools, *in situ* transmission electron microscopy (TEM) has taken a prominent place[3-6].

Ever since the development of electron microscopy in the 1930s, there has been efforts to add external stimuli and increase the time resolution in studies of materials as they transform. Using specialized holders and microscopes, a wide range of physical and chemical stimuli have been integrated into TEM, such as electrical and electrochemical biasing, temperature control via heating/cooling, and exposure to liquids, gases, and light[5]. Under the influence of these triggers, material structure and properties evolve on timescales ranging from femtoseconds (10^{-15} s; fs) to seconds, or longer (FIG. 1). For example, charge transfer upon photoexcitation takes place on ultrafast, fs-to-picosecond (10^{-12} s; ps) timescales[7]. On the other hand, thermally-induced phase transitions in nanoparticles may take seconds or longer[8-10] technical improvements such as the

development of sensitive and fast detectors and the integration of pump–probe techniques have advanced *in situ* TEM to a degree where time-resolved studies are now possible on a vast range of timescales while maintaining atomic-scale spatial resolution. Compared to time-resolved X-rays[11-14], the TEM offers a particularly versatile and relatively cost-effective platform that combines imaging, diffraction, and spectroscopy within a table-top setup that does not require large facilities, such as synchrotrons and free-electron lasers. The latter have the advantage of exceptionally high brightness, relatively low repetition rate, and, as a consequence of the lower absorption cross-sections of X-rays, the possibility to routinely work with bulk liquids and solids. The TEM platform, on the other hand, allows the study of dynamics on the level of individual nanoparticles and a range of timescales and enables the discovery of temporal dynamics and size- and shape-dependent behavior that is otherwise hidden from conventional, bulk-level studies that involve ensembles of nanoparticles[15-17].

This Review discusses recent key advances in time-resolved TEM and its application to the study of nanoscale dynamics of chemical processes on a broad range of timescales. Examples include phase transitions, energy or charge transfer, nanoparticle restructuring, and nanomechanical motion. We particularly focus on the recently emerged field of ultrafast pump-probe TEM that enables investigations of photoinduced dynamics with temporal resolution down to hundreds of fs[18-23]. We also emphasize the unique capabilities of single-nanoparticle-level probing of dynamics. This Review only briefly describes *in situ* TEM holders and their use for the study of materials dynamics in the liquid phase, which has been covered elsewhere[24]. The fast-developing fields of 4D scanning TEM[25] (STEM) and environmental STEM[26-27] are outside the scope of this Review.

Time-resolved TEM instrumentation

Early examples of time-resolved TEM sought to explore how materials behave when irradiated by high-energy particles, *i.e.* electrons, to understand mechanisms of damage of structural materials, for example, in nuclear reactor environments[28]. Ever since, the available stimuli in TEM have been expanded and now include exposure to gaseous/liquid reactants, heating and cooling, electrochemical biasing, light illumination, magnetic fields, or mechanical stimuli. Further, the electron beam inherent to the TEM has been used to deliberately trigger processes other than just radiation damage, for example local heating or chemical reduction, which allows the stimuli and structural evolutions prevalent *in operando* (during operation) to be mimicked[8,29].

In situ TEM techniques often require the use of specialized holders or cells. Gas/liquid environments are most commonly created using enclosed cells[30,31] or by trapping liquids between layers of graphene[32]. The closed-cell design enables the use of flow or the coupling with auxiliary features such as heating elements, with the drawback of compromised spatial resolution due to the relatively thick cell and windows. On the other hand, a graphene-based liquid cell provides better spatial resolution and capability for full three-dimensional (3D) imaging of nanostructures in solution[33], at the cost of ease-of-use, confinement/substrate effects in the thin sheet of liquid, and nonuniformity of the encapsulated liquid pockets[34]. A sample can be heated with a furnace-type heating holder or with a precise micro-electro-mechanical-systems (MEMS)-based heating holder[35,36]. The latter offer faster and more uniform sample heating than older furnace-type holders and is becoming the preferred standard. *In situ* exposure of the specimen to electromagnetic radiation (from ultraviolet to radio waves) is accomplished with sample holders equipped with optical fibers[37-40] or waveguides[41-43], by planting light-emitting diodes directly on the holder tip[44], or via preexisting ports in the microscope column and free-beam laser optics[19,21,45,46]. The latter

has the advantage of being able to accommodate a larger range of tunability of the irradiation wavelength and incident photon densities at the sample, while requiring more elaborate laser systems and optical setups. Luminescence emitted when electrons impinge on a sample, called cathodoluminescence, can be collected using holder-based parabolic mirrors[47]. Finally, holders with piezo-controlled tips can be used to apply mechanical forces to a sample or to complete a circuit to study a nanobattery *in operando*[48,49].

All systems in nature and technology are driven continuously out of equilibrium by the exchange of energy with the environment. A survey of the literature shows that time-resolved TEM has been used for atomic-scale probing of two classes of processes in which materials are driven away from equilibrium under the action of energetic stimuli and/or environmental conditions: i) the transport of energy, charge, spin, and/or quasiparticles (*e.g.*, phonons), which has time constants in the fs to microseconds (10^{-6} s; μs) range and ii) structural re-organization spanning a crystallite, which is often limited by atomic diffusion and/or nucleation barriers and takes typically place on the milliseconds (10^{-3} s; ms) to seconds or longer timescale. Both classes of processes are of central importance to the properties and function of molecular and solid-state materials. The former class typically requires a pulsed trigger and probe of sufficient, *i.e.*, fs to μs, time resolution; on the other hand, the latter types of processes are studied under a constant, continuous perturbation by exploiting the ms-or-better frame times of imaging cameras. We describe the respective instrumentation, the accompanying spatial and temporal resolutions, and technical limitations encountered.

Slow dynamics under constant perturbation

A majority of time-resolved TEM studies involves relatively slow dynamics on the ms or longer timescales under constant perturbation, such as shape evolution of nanoparticles[50-54]. A constant perturbation is applied to the sample with continuous imaging to track its evolution (FIG. 2a). These studies are amenable to all types of *in situ* stimuli that can be applied continuously and uniformly, *e.g.*, constant-pressure gas exposure, electrochemical bias, lighting, or heating/cooling. Since they are performed with continual imaging, the achievable temporal resolution is primarily limited by the rate at which data can be recorded by the electron detector, *i.e.*, the frame rate. Consequently, these experiments have greatly benefitted from the recent development of fast detectors.

The fields of materials and biological electron microscopy have been revolutionized by the development of direct-electron detectors[55-57]. Whereas conventional charge-coupled device (CCD) cameras detect electrons only indirectly via a scintillator and fiber optics, the sensor of a direct detector is radiation hardened to allow it to be exposed directly to high-energy electrons. Several implementations for direct-electron detection exist, such as active-pixel, hybrid-pixel, and pn-type CCD-based sensors[58-60]. Monolithic active-pixel sensors are capable of recording single-electron events[61,62], and their spatial resolution and signal-to-noise ratio are significantly enhanced over indirect detectors[61,63]. Most importantly, the highest full-frame rates achieved with such detectors amount to 87 kHz[64], pushing the time resolution of TEM experiments conducted under constant perturbation into the μs regime, while typical speeds amount to several kHz. This represents a thousand-fold improvement in temporal resolution compared to conventional CCD cameras. However, as frame rate increases, the number of detected electrons per frame decreases, which

reduces the achievable contrast in the image. Studies have suggested that electron current starts to affect image quality for exposure times under 100 μs[59.60].

The developments in direct-electron detector technologies are particularly promising for time-resolved electron energy loss spectroscopy (EELS) inside the TEM. EELS is capable of capturing interfacial chemical composition and bonding, charge transfer dynamics, or spin-state changes that are triggered by external stimuli[65-70]. While direct-electron detection in imaging and diffraction has led to many successes so far, the potential of time-resolved spectroscopy has only recently been demonstrated[58,71,72].

In a notable recent experiment using fast detectors, a high-sensitivity delay-line detector was used for the imaging of magnetic vortex gyration with a temporal resolution of ~100 ps and continuous irradiation with a microwave magnetic field at GHz frequencies[42]. These experiments profited from synchronized triggering and detection, and the reversibility of the dynamics, which enable the averaging of many frames with low counts to build up sufficient contrast in the final image. The concept of probing material responses to harmonic excitations (*e.g.*, microwaves and radio waves) at high temporal resolution down to fs can also be achieved using electron-beam chopping schemes, which will be discussed later in more detail[43,73,74]. Besides delay-line detectors[75], other event-based technologies such as the Timepix detector[76] hold great promise for pushing the time resolution into the ps regime.

The tremendous improvements in spatial resolution, sensitivity, and temporal resolution of electron detectors put considerable constraints on the ability to handle, transport, and process large amounts of data. This issue becomes especially problematic in time-resolved TEM imaging experiments where rare events, such as surface reconstruction[77] or nanoparticle rotation[78], make up only a very small fraction of all frames recorded. Recently, new computational approaches have

emerged to extract relevant information from data-intensive imaging experiments[79]. These include machine learning[71,80] and compressed sensing[81-83].

Dynamics induced by pulsed excitation

Pulsed energetic excitation is commonly used to drive a material far away from its equilibrium state and its subsequent evolution back to an equilibrium state is probed in a time-resolved manner, gaining valuable information on charge, energy, spin, mass transfer, and relaxation processes on timescales ranging from fs to μs. In pump–probe electron microscopy, a short excitation pulse (the "pump") triggers the dynamics in the sample, while a fast camera (FIG. 2b1) or short electron probe pulses (FIG. 2b2-4) capture snapshots of the dynamics at later times as the material returns to the ground state or to a new (meta)stable state. By systematically varying the relative time delay (Δt) between the pump and the probe, a movie of the ensuing materials dynamics is recorded. Since these studies require short excitation pulses, the range of useful stimuli is more limited than with studies of slower dynamics under constant perturbation (FIG. 2a). Common triggers for driving a system away from equilibrium include short laser pulses[84], electrical pulses[49,85,86], pulses of strain[87], or rapid temperature changes, *via* either MEMS-based heating holders[88,89] or photothermal heating with a pulsed laser[16,17,65,90,91]. The combination of fast direct-electron detection cameras, described in the previous section, with such triggers has the potential to uncover irreversible dynamics on the μs-to-ms timescale; yet this field has been largely unexplored. Perhaps this is due to the combination of rather low counts per frame and the need for large material changes to be induced by the trigger, in order for obtaining sufficiently high signal-to-noise ratio in the final images.

Higher temporal resolution can be obtained by using short pulses of electrons for probing. The temporal resolution is then determined by the convolution of the pump and probe pulses, as well as their relative "jitter", *i.e.*, slight, random phase shifts in the arrival times of the pulses. Two main schemes for the generation of short electron pulses in TEM have emerged: (1) photoemission and (2) beam blanking[92]. In the former, a short (fs–μs) UV laser pulse impinges on a photocathode located in the gun of the electron microscope. Electrons are emitted either by means of the photoelectric effect in a thermionic cathode[84,93-98], or by means of laser-triggered field emission[46,99-101]. In the latter, the electron gun of the microscope is unaltered; the continuous electron beam is chopped into short pulses by sweeping it at a high speed over a narrow slit inserted in the main column of the electron microscope before the sample. The choice of source largely determines the achievable electron pulse properties such as energy spread, pulse duration, repetition rate, and coherence, which is a measure of the correlation between the phases of electron waves and determines how well they can interfere with each other.

The dynamics induced by the pump pulse can be *irreversible*, when the initial and final states are different, or *reversible*, when the material returns to its initial state after excitation. This distinction has important ramifications for the implementation of the pump–probe technique and the temporal, spatial, and energy resolutions achievable in the experiment, as discussed below. Techniques that can probe irreversible dynamics can commonly also probe reversible dynamics. However, the reverse is not the case.

In *single-shot TEM* (FIG. 2b2) an electronic or structural material is triggered by a short pump pulse and a snapshot of the ensuing dynamics is probed by a single, intense electron pulse at a slightly later time. This technique has been used to probe laser-induced irreversible processes such as amorphization and crystallization pathways of individual perovskite nanoparticles[91], phase

propagation in reactive multilayer foils[90], and carbothermal reduction of metal oxide nanoparticles[102]. The electron probe pulse must contain a sufficient number of electrons (>10^6–10^7)[19,92] to obtain an image, diffraction pattern, or energy-loss spectrum with sufficient signal-to-noise ratio in a single shot. This presents a major challenge since electrons repel each other, which leads to lengthening of the pulse, increased energy spread, and decreased coherence. These electron Coulomb repulsion effects thus directly compromise the quality of the acquired data and the achievable time resolution[103]. Furthermore, due to the rather low quantum efficiencies of typical photocathode materials, sources for single-shot TEM are often operated close to their damage threshold and need frequent replacement[104]. In addition, only one time delay is sampled per pump–probe measurement. In order to capture the complete transition of the material on a broader range of timescales, many pump–probe measurements with different time delays need to be repeated on different parts of the sample, which poses significant constraints on the reproducibility of the process and the homogeneity of the sample. In light of these technical challenges, single-shot pump–probe TEM has achieved a typical spatial and temporal (*i.e.* spatiotemporal) resolution of tens of nm and a few nanoseconds (10^{-9} s; ns)[19,93,105]. Combined optimization of spatial, temporal, and energy resolutions can be achieved by tuning the UV laser pulse length and intensity at the cathode, as well as the bias of the electron gun. In this way, an energy resolution of ~2 eV was obtained for single-shot EELS on the ns timescale[102,105]. The throughput of the microscope column can be increased by the insertion of an additional magnetic lens after the electron gun[93,94,105,106].

In the above cases, the electron pulses are generated by photoemission from large and flat cathode tips made out of robust thermionic materials, such as lanthanum hexaboride or tantalum[92]. Recently, a flashed Schottky field-emission tip was used for single-shot atomic-scale imaging with

μs electron pulses[91]. Furthermore, radio frequency (RF)-based electron guns are employed to generate relativistic (MeV) electron pulses with reduced Coulomb repulsion effects enabling single-shot imaging and diffraction with resolutions in the ps regime[107-112]. RF technology has also lead to impressive developments in dedicated ultrafast electron diffraction setups for single-shot studies with fs temporal resolution[113-117].

The constraint on sample homogeneity in single-shot methodologies for irreversible dynamics is partially alleviated in *movie-mode TEM*[19,118,119] (FIG. 2b3). This technique is enabled by a burst of intense ns–μs electron pulses impinging on the sample after applying a trigger, and a synchronized downstream beam deflector that directs each electron pulse onto a separate portion of the camera. In this way, a short movie of up to sixteen subframes is recorded for each sample location[19]. Control over the relative spacing between laser pulses allows probe pulse trains to be tailored to best match the intrinsic response time of the excited material. This is a large advantage compared to single-shot TEM since many processes in chemistry do not unfold exactly the same way in every shot. Since the deflected images and patterns are demagnified before they are projected onto the camera, the detector pixel size and point-spread function may become a limiting factor for the contrast and resolution. Typical spatiotemporal resolutions amount to tens of nm and tens of ns. Time delays of up to hundreds of μs can be covered. This methodology has been successfully applied to study laser-induced melting and solidification phenomena in thin-film alloys[120], *in situ* reactions of individual nanothermite nanoparticles[121], nucleation and growth dynamics in thin-film phase-change memory materials[122], and thin film recrystallization[123]. Recently, fast electrostatic beam deflectors have also been used to effectively multiply the intrinsic frame rate of the electron camera[82,83].

Single- and multi-shot implementations of pump–probe TEM are limited by the Coulomb repulsion effects in the intense electron bunches used to take snapshots of irreversible processes. Much higher resolution can be obtained using stroboscopic approaches; however, a prime caveat is that the process induced by the pump pulse needs to be reversible, *i.e.*, the material needs to recover to its initial state between two pump pulses. In *stroboscopic TEM* (FIG. 2b4), the spatiotemporal resolution is improved by maintaining a low number of electrons per probe pulse (~1–100 electrons/pulse) mitigating Coulomb repulsion effects. The lower counts are compensated by employing high pump-probe repetition rates (kHz–GHz) and accumulating many (~10^4–10^9) pulses onto the detector per time delay. In this way, atomic-scale resolution (2–3 Å) images were acquired using fs-ps electron pulses at MHz-GHz repetition rates[95,124]. We note, however, that several claims of atomic-scale resolution using pulsed TEMs in the literature[46,101,125,126] lack the report of parameters such as repetition rate and/or pulse length, or they do not show the actual image from which spatial resolution was inferred. Furthermore, these experiments were conducted without the presence of a pump laser on the sample, which can cause significant sample drifts and vibrations, compromising the imaging resolution in pump–probe fs TEM experiments. In studies where a laser is used for excitation[127,128], practical spatial resolutions in the nm range have been reported.

The electron pulses in stroboscopic TEM are commonly generated using photoemission cathodes excited by high-repetition-rate laser systems[92]. In particular, nanoscale field-emitters have demonstrated superb brightness characterized by a combination of large coherence and short pulse length, while the overall beam current under such conditions is generally low, which necessitates the use of higher repetition rates[46,99]. Other techniques such as microwave compression[114,129], terahertz compression[130,131], RF optics[132,133], or photon gating[134,135] have been

proposed to further optimize and control electron bunch properties and extend the resolution into the deep fs regime. Applications of stroboscopic TEM using photoemission sources include the study of rapid laser-induced phase changes in (nano)materials[16,17,102,123,136-138], observation of nanodroplet, nanobubble, and nanomotor dynamics in liquids[100,139-141], and the visualization of evanescent fields, plasmon-polaritons, and plasma dynamics[69,84,142-148].

Laser-free implementations of stroboscopic TEM (and SEM) have been developed as early as the 1960-70ies[149-152]. In recent years, this form of probing has experienced renewed interest[19]. The main advantage of these implementations is that no modifications of the electron source are required. Instead, an electrostatic or RF-based beam blanking device is inserted in the microscope column; this device deflects the electron beam rapidly over a fixed aperture thereby chopping the beam in short pulses[43,73,74,85,92,124,153,154]. This approach effectively preserves the brightness and energy spread of the native source, and switching between pulsed and continuous emission modes is especially straightforward. Currently, a temporal resolution of ~100 fs has been demonstrated with this approach, albeit not implemented in a TEM[155]. The intrinsically high (GHz) repetition rate bears the advantage of high duty cycles (~10–20%; fraction of electrons used) and shorter integration times necessary to obtain data with sufficient signal-to-noise ratio; on the other hand, the GHz repetition rate also limits the scope of materials that can be studied in pump–probe studies since excited-state lifetimes need to be in the ns range. So far, laser-free stroboscopic TEM has been demonstrated with harmonic excitation of the sample in the field of electrodynamics[43] and magnetization dynamics[42,150]; studies with other triggers particularly useful in chemical dynamics (*e.g.*, visible light irradiation or heating) are expected to emerge in the coming years. These new technologies thus offer a plethora of application opportunities to unravel magnetic, plasmonic, and excitonic dynamics in advanced functional materials[74].

The use of pulsed electron beams generated in a laser-free TEMs have also been explored for the mitigation of radiation damage in beam-sensitive materials, such as polymers, biomaterials, and hybrid organic–inorganic perovskites[156,157], and to reveal new structures of materials at high resolution[158].

Pump–probe stroboscopic TEM is not limited to the ultrafast (fs) regime. Both photoemission and laser-free concepts allow for ample tunability of the electron pulse properties. The longer the electron pulse, the more the number of electrons that can be contained in the pulse before Coulomb repulsion effects dominate, and the lower the repetition rate necessary to obtain sufficient contrast in a reasonable integration time. Low repetition rates allow for longer recovery times of the sample after excitation, which opens up studies of charge recombination processes or phase transitions with excited-state life times in the tens of μs or ms timescale[16,159,160]. In this regard, the combination of pulsed electron sources and sensitive direct-electron detection cameras allows repetition rates to be pushed down while maintaining sufficient temporal resolution and image quality at reasonable integration times[96].

In addition to the main methodologies for time-resolved TEM depicted in FIG. 2, hybrid technologies, combining two or more schemes, are emerging. For example, combining fast direct-electron detector gating (FIG. 2b1) and electrostatic beam deflection, such as in movie-mode TEM (b3), enables stroboscopic pump–probe TEM of repeatable processes (FIG. 2b4) on the ~100 ns timescale without the need for the generation of short electron pulses with lasers[161]. Another example constitutes the implementation of a fast deflector (FIG. 2b3) inside an EEL spectrometer to sweep the electron beam across the camera following the application of a trigger to the sample. The temporal evolution of the material is imprinted in the time profile of the scattered electron beam, which is projected onto the camera by deflection. This streak-camera approach can be

implemented for time-resolved imaging, diffraction, or spectroscopy in single-shot (FIG. 2b2) or stroboscopy (FIG. 2b4) modes using a continuous or pulsed electron source. This approach has achieved temporal resolutions in the hundreds of ns range with considerable promise for further improvements in resolution down to the ps timescale[83,162,163]. Finally, the synchronization of pulsed electron beams (FIG. 2b2-4) and/or beam deflectors (FIG. 2b3) with fast direct-electron detectors (FIG. 2a and 2b1) could help in minimizing distortions and artifacts due to the rolling-shutter problem[82,164].

Applications of time-resolved *in situ* TEM

The technical advances described in the previous section have transformed *in situ* TEM into a powerful tool for studying chemistry in real-time on the nanoscale, as aptly demonstrated by the plethora of recent *in situ* studies that have exploited the unique capabilities of TEM over other techniques[32,165-167]. We identified four areas in which dynamic *in situ* TEM shows great promise: crystal phase transformations, charge- and heat-transfer dynamics, restructuring of nanoparticles, and nanomechanical motion. While our selection of examples does not exhaustively cover the entire field, it is meant to showcase the breadth of timescales that can be covered using the techniques presented in the previous section. Wherever possible, a reference to the respective method in FIG. 2 is made for each example.

Microscopic origins of phase transformations

Crystal phase engineering enables us to grow nanostructures with controlled phases (namely, the arrangements of atoms in crystals) exhibiting superior functional properties compared to bulk materials[168]. The phase change may involve a transition between two states of matter, *e.g.*, liquid

and solid, or a transformation between two different solid-state crystal structures of the same material, under the influence of a temperature change, electric field, light, stress, or ionic radiation. The transition temperature and the mechanism—the starting, intermediate, and end-point structures as well as the routes by which they transform—of phase changes critically depend on the presence of interfaces, defects, and strain and can therefore be significantly different for nanoscale materials as compared to their bulk counterparts[10]. *In situ* time-resolved TEM has become an indispensable tool to understand these intricate phenomena because they can capture intermediate atomic-scale structures in the course of a transformation from one phase to another on timescales ranging from fs to minutes. In the following, we highlight several examples in which time-resolved TEM has led to the discovery of new transient/metastable nanoscale phases and transformations, insights into how external stimuli can be used to control phase changes, and the elucidation of atomistic dynamics that determine the nucleation and growth of a new phase.

Steady-state transformations. A large body of recent literature reports on the use of *in situ* TEM for studies of phase transitions (FIG. 2a) of nanoscale materials induced by heat[52,169-171] and electrical bias[172-174] with respective applications in catalysis—by combination with gas exposure of the specimen—and battery research—by combination with liquid exposure of the specimen[10]. In many of these studies, the effects of the electron beam need to be carefully controlled and disentangled from other stimuli[4,175]. In some cases, however, the electron beam is deliberately used to induce the phase transformation, either by means of the temperature increase resulting from electron impact or through ionization processes themselves, or by a combination of both effects and other stimuli[8,176-178].

For example, Heo *et al* studied the electron-beam-induced transition of copper selenide nanoparticles from a low-temperature, ordered phase to a high-temperature, superionic phase with a liquid copper sublattice[8] (FIG. 3a). Real-space and real-time imaging of this process at the single nanoparticle level provided direct insight into where new phases nucleate and how they grow. Nucleation of the high-temperature phase most often occurred at sites in the crystal with low atomic coordination and therefore lower activation energy for the phase transition. Dionne and coworkers have done similar studies on photocatalytic dehydrogenation of Pd nanostructures under simultaneous light and gas exposure[39,167]. In this work, individual Pd nanostructures located in the vicinity of plasmonic gold nanoantennae were imaged by TEM in the course of their dehydrogenation. The change from the hydrogenated to the dehydrogenated phase was captured by recording changes in lattice spacing of the Pd over time (seconds). The phase nucleation behavior was found to be affected by the proximity, and therefore the strength of coupling, between the Pd structure and nanoantennae. Plasmonic coupling promoted nucleation at energetically unfavorable sites compared to spontaneous dehydrogenation, which demonstrated the role of the nanoantennae in catalyzing dehydrogenation[39,167]. Finally, a remarkable study captured the nucleation and growth of NaCl crystals inside carbon nanotubes with atomic resolution on the ms time scale[179]. This achievement demonstrates the capability of fast TEM detection for probing intriguing transient phenomena on the nanoscale.

Non-equilibrium phase transitions. Critical ephemeral processes underlying phase transitions, such as nucleation and growth phenomena and localized phase competition, are difficult to reveal by probing under constant perturbation with limited temporal resolution and that are spatially averaged over many phase-separated regions. *In situ* TEM techniques with increasingly high

temporal and spatial resolution (FIG. 2b) have been used to directly visualize localized structural changes in real-time opening up new avenues for the study of nanoscale non-equilibrium processes induced by stimuli.

For example, amorphization and (re)crystallization kinetics after rapid temperature jumps applied through MEMS-based heating holders or indirectly *via* short laser pulses have been reported[88,90,123]. Sohn *et al* used a sample holder, capable of rapid heating, and a fast detector to reveal the dynamics of recrystallization in metallic glass nanocolumns with sub-second resolution[88] (FIG. 2b1). In small diameter columns, only a single nucleation event was possible due to the diameter constraints leading to a single-crystalline morphology outcome; whereas in large diameter columns, multiple nucleation events took place resulting in a polycrystalline outcome. Photothermal heating, namely the temperature increase resulting from the dissipation of absorbed photon energy, offers a particularly attractive way to impulsively heat materials *in situ* with rates as high as 10^{11} K/s[180]. In particular, Xiang *et al* demonstrated the non-equilibrium conversion of amorphous silicon to single-crystalline silicon using localized photothermal heating achieved with a fiber-optic near-field probe[181]. Furthermore, using single-shot (FIG. 2b2) and movie-mode (FIG. 2b3) probing techniques, ns-resolved snapshots of melting and solidification processes in perovskite nanocrystals[91], metal oxides[123] and phase-change materials[120,122] have been acquired. Similarly, single laser pulses have been used to trigger irreversible chemical transformations[17,90,102,122,182] and Coulomb fission[183] inside the TEM. Such experiments can be combined with nanocalorimetry measurements inside the TEM to capture concurrent enthalpic changes[184]. For example, Sinha *et al* revealed an intermediate liquid Ni phase in the irreversible carbothermal reduction of polycrystalline NiO films[102]. They used single-shot electron diffraction and EELS to track the structure and composition on the μs time scale (FIG. 3b). These

investigations demonstrate that the nucleation and propagation of new phases in nanoscale materials critically depend on the defect structure and presence of interfaces, which are not accessible in bulk measurements. Such atomic-scale investigations lay the foundation for crystal-phase engineering of functional nanomaterials, which are, for example, more robust towards thermal degradation.

Finally, with pump–probe TEM (FIG. 2b4) the study of phase transitions has been pushed into the ultrafast temporal regime (fs–ns) revealing intriguing phenomena such as nonthermal melting[185], metal-to-insulator transitions[136,186], and spin-state switching[16,187]. In a remarkable recent study, Danz *et al* used ultrafast TEM for real-space imaging of charge-density wave (CDW) phase dynamics with nm spatial and fs temporal resolution in a two-dimensional (2D) material[138] (FIG. 3c). They employed a customized aperture array to obtain dark-field images with enhanced contrast to track the evolution of non-commensurate (NC) and incommensurate (IC) phase domains in TaS_2. These studies demonstrate the power of ultrafast TEM to explore optical control over physical and chemical properties of nanoscale materials for applications in data storage devices, high-speed detectors, photonic circuits, and energy conversion.

Charge/heat transfer dynamics and imaging evanescent fields

The storage and transfer of energy in the form of charges (electrons or ions) or heat plays an increasingly important role in today's consumption society. The atomic-level understanding of how energy localization and transfer depend on the structure, composition and bonding of a material is paramount for the rational optimization of energy conversion systems[188,189]. In this section, we showcase the role of time-resolved TEM tools for the study of charge dynamics in (photo)electrochemical materials[7,190-197], the visualization of plasmonic evanescent

fields[142,143,147,198] and plasmas[84,148], and the dynamics of phonons (carriers of vibrational energy) after light excitation[126-128,199-205].

One specific area that has greatly benefitted from time-resolved TEM is battery research[188,190,191-197,206,207]. We focus here on novel solid metal-air batteries[208]; *in situ* TEM studies of solid–liquid battery systems have been covered elsewhere[24]. Time-resolved imaging, diffraction, and spectroscopy in the TEM can uncover the diffusion of ions, the formation of electrochemical reaction products, and probe the reversibility of the charging–discharging cycle. Operational solid-state nanobatteries have been built by integrating cathode and anode, separated by an appropriate electrolyte, within a dedicated biasing holder and exposing the electrodes to gases in an environmental TEM[192].

Alkali metal–air (CO_2/O_2) batteries have theoretical energy densities that are much higher than those of lithium-ion batteries[208]. They are therefore considered to be a potential solution towards next-generation electrochemical energy storage for applications such as electric vehicles or grid energy storage. However, these battery systems are still in their infancy, due to limited capacities and low cyclability. *In situ* TEM have recently played an important role in shedding light on some of these challenges. In one study, Han *et al* sought to investigate how CuS behaves as a potential cathode material in a Na–O_2 battery[190]. It was found that when in contact with sodium metal, sodiation of a CuS nanocolumn produced a Na_2S structure with embedded Cu nanoclusters. These clusters were postulated to act as catalysts for oxygen reduction, necessary for rapid battery cycling, thus rendering this an effective cathode material. Fast TEM (FIG. 2a) enabled real-time tracking of the sodiation process (FIG. 4a top). Likewise, Gutierrez-Kolar *et al.* studied the sodiation of a SnSb cathode under bias, imaging the propagation of the sodiated phase to understand its charge–discharge kinetics[197] (FIG. 4a bottom).

The elemental specificity of core-level EELS renders it especially powerful in the tracking of charge/ion dynamics inside (photo)electrochemical materials[65,69,192,195,196]. As notable examples in the ultrafast time domain, pump–probe EELS (FIG. 2b4) has been used to track charge carrier dynamics and trapping in hematite nanocrystals[7] and the energy gap shrinkage in graphite thin films[65]. On the other hand, in the low-energy inelastic loss region, ultrafast EELS enabled the imaging of evanescent plasmonic fields in the vicinity of nanostructures[143,144,198,209-212]. The ability to localize and enhance electromagnetic fields by plasmonic nanomaterials have been widely used in, for example, biological sensing, surface-enhanced Raman scattering (SERS), photothermal therapy, or solar energy conversion[213-215]. By carefully overlapping femtosecond laser pump and electron probe pulses in both space and time inside an ultrafast TEM, the imaging electrons can couple with photons in the laser excitation pulse. The electrons, with energies typically on the order of 200 keV, absorb/emit integer numbers of photons, which can then be used to directly visualize the scattered evanescent field surrounding the nanostructure. This technique has been dubbed photon-induced near-field electron microscopy[142] (PINEM). Recently, it has been used to directly visualize the local plasmonic coupling between single Au nanocapsules and graphene step edges on the nanometer scale[143] (FIG. 4b). The authors found that the plasmonic field of the Au nanostructure is significantly modified by the presence of the graphene edge step originating from an asymmetric surface charge density at the tips of the nanocapsules. This effect could be tuned by a change in the tip–edge distance and the relative light polarization direction. Similarly, PINEM was employed to probe phonon–polariton wavepacket dynamics in photoexcited 2D materials on the fs time scale[147]. Phonon–polaritons are lattice vibrational modes coupled to electromagnetic waves, and play a role in optoelectronic and photonic applications that rely on the spatiotemporal control of light[216].

The transfer of energy in the form of heat is of great importance in a large variety of applications such as fast data storage, personal electronics, and alternative-energy technologies[217-219]. The embodiment of heat inside materials are phonons—collective vibrations of atoms inside a lattice—that propagate on a timescale dictated by the speed of sound in matter, which is on the order of 1000 m/s (*i.e.* 1 nm/ps). Ultrafast TEM (FIG. 2b4) with ps temporal resolution therefore offers a unique way to capture phonon transport through nanoscale materials[127,128,199-205,220,221]. Flannigan and co-workers have tracked coherent phonon dynamics following pulsed laser excitation in a variety of materials revealing how nanostructure affects phonon nucleation and propagation[199,201]. For example, they imaged photoexcited strain-wave dynamics in bilayer transition metal dichalcogenides[201] (FIG. 4c). It was found that few-layer crystal step edges and terraces allow for increased freedom of motion relative to regions far from the defect, causing the preferential excitation of intra-layer phonon modes at free basal-plane edges and dephasing of vibrations between the layers. These results uncover the basic physical processes at the heart of thermal-energy transport and illustrate the critical influence of defects on the emergent optoelectronic properties of materials.

Restructuring dynamics of individual nanoparticles

Unique compared to most other structural probing tools, TEM has the powerful capability of being able to image the behavior of individual nanoparticles. This is particularly important in the field of catalysis where it is known that materials undergo atomic-scale rearrangements that may lead to activation or passivation of the catalyst during operation[222]. Only by studying nanoparticles one-by-one under realistic working conditions, detailed structure–property–function correlations can be made, which enable the optimization of catalytic activity by precise understanding and control

of the size, phase, composition, strain, and morphology of the catalyst. In this section, we present some notable examples of the use of time-resolved *in situ* TEM to the probing of single-nanoparticle restructuring dynamics in the field of (electro)catalysis[223]. These experiments require high spatial resolution (<0.5 nm), but only moderate temporal resolution (ms–s), which renders fast-camera imaging methods (Fig. 2a) most suitable.

Despite intensive research efforts, the identity and nature of the active sites for gas molecule (O_2, CO, CO_2, H_2) adsorption/dissociation by supported metal nanoparticles is still an unresolved issue in heterogeneous catalysis. This stems from the lack of a clear picture of the structural evolution of the metal nanoparticles and the metal–support interface at near reaction conditions, *i.e.,* under gas exposure at high temperatures and pressures. Using time-resolved TEM, dynamical behavior, such as surface (re)faceting[50-54], disordering[40,77,224], segregation[1,224-227], shell and void formation[225,226-229], nanoparticle rotation and tilting[78,230], and coarsening[52,231] have been observed. For example, Vincent *et al.* reported dynamic fluctuations occurring at and near Pt–CeO_2 interfaces during CO oxidation[230] (FIG. 5a). Using a fast direct-electron-detection camera[232], the authors were able to correlate catalytic turnover frequency with the destabilization of the Pt particle, an enhanced rate of oxygen vacancy creation and annihilation, and increased strain at the CeO_2–support interface. The lack of lattice fringe contrast in the image of the supported Pt particle indicates that it is undergoing dynamic restructuring at a speed that is much higher than the frame rate of the camera. Similarly, He *et al.* imaged the size-dependent reconstruction dynamics of single Au nanoparticles on CeO_2 upon exposure to reactant gases (CO + O_2)[77]. They found that, while large Au nanoparticles remain rigid, ultrasmall Au clusters lose their intrinsic structures and become disordered during catalysis triggered by the adsorption of gas molecules at the surface.

In many cases, significant (re)faceting, *i.e.*, the (de)stabilization of crystallographic planes at the nanoparticle surface, is observed under reaction conditions[50-54]. Refaceting is caused by changes in the surface energy through adsorption of gas molecules, which in turn affects the catalytic activity of the nanoparticles. This has been captured by Vendelbo *et al* for Pt nanoparticles during CO oxidation[53]. Using a TEM holder-based nanoreactor and microkinetic modeling, the authors were able to correlate the dynamic and reversible refaceting of Pt nanoparticles[53] (FIG. 5b) with the oscillatory CO oxidation reaction kinetics. In another example, significant changes in the surface structures of TiO_2 anatase nanocrystals were observed under exposure to water and UV light[40]. The initially crystalline surface of the nanoparticles becomes amorphous during the photocatalytic water splitting reaction. This process results from the loss of O^{2-}, which produces vacancies in the material that act as sites for binding water molecules to the surface of the nanoparticles (FIG. 5c). Similar behavior has been reported to take place during the electrocatalytic water oxidation on Co_3O_4 nanoparticles[233].

Catalysis and battery chemistry often involve ion diffusion in the presence of liquids. In recent years, tremendous progress has been made in the development of suitable holders for conducting *in situ* TEM experiments in wet phases[24,174,234-236]. This has enabled, for example, the elucidation of intermediate structures during dynamic nanoparticle growth processes[32,166] or void formation inside nanoparticles[226,228,238,239]. Using a fast complementary metal-oxide semiconductor (CMOS) detector and a silicon nitride liquid cell, Chee *et al*. tracked the hollowing of Ag nanocubes via the nucleation, growth, and coalescence of voids during a galvanic replacement reaction with Au^{3+} from solution[228] (FIG. 5d). This process, known as the nanoscale Kirkendall effect, arises from unequal diffusion rates between two atomic species leading to void

formation near the interface[240]. Hollow nanoparticles have been suggested to exhibit enhanced catalytic performance compared to solid nanoparticles[241].

Clearly, the above examples demonstrate that the shape, composition, or structure of a nanoparticle under working conditions may largely differ from those under static conditions. In fact, nanoscale materials continuously undergo rapid transformations, which necessitates the use of tools with the appropriate spatiotemporal resolution critical to disentangle these complex processes. The rapid technological developments in the field, and related fields such as environmental STEM[242-246], have thus established time-resolved *in situ* electron microscopy as an essential characterization tool in electrochemistry and heterogeneous (photo)(electro)catalysis.

Nanomechanical dynamics

Nanoscale materials have unique properties mainly due to their large surface-to-volume ratios. Besides differences in optical, electronic, and magnetic properties compared to the bulk, the unique mechanical properties, *e.g.* hardness, stiffness, elastic modulus, surface energy, of nanomaterials allow for novel applications in many fields, such as tribology, coatings, surface and strain engineering, and nanomanufacturing[247,248]. For example, nanoscale materials can often accommodate strain and stress better than their bulk counterparts[249]. Furthermore, particle movement is governed by adhesion, friction, gravitation, and viscous flow forces, which act differently on the nanoscale[141,250,251]. In order to guide predictive theories and achieve real control over the functionality of nanostructures for integration in devices, *in situ,* time-resolved structural probing tools, such as TEM, are becoming indispensable. In this section, we highlight several examples where the increased spatiotemporal resolution of TEM has led to new insights into the mechanical behavior of nanoscale materials.

In situ nanomechanical testing combined with fast-camera TEM imaging (FIG. 2a) offers the ability to observe in real time the dynamics of defects, such as dislocations and twins, while quantitatively correlating their behavior with an applied stress[252-256]. For instance, Kiener *et al* studied the deformation of an ion-irradiated Cu nanocolumn under continuous compressive strain in order to understand how radiation-induced defects affect the mechanical properties of the nanocolumn[252]. They found a transition length scale of ~400 nm, below which the yield strength becomes dislocation-source-limited. The technique has also been used to unveil the mechanistic origins of twin boundary formation in magnesium nanopillars, providing insight into defect formation under load[256]. Further, by combining nanomechanical testing with localized laser heating[253], these techniques can be extended to the characterization of mechanical properties of materials in extreme environments or high-temperature applications.

As the size of a material is reduced to the nanoscale, the timescale of mechanical motion extends into the ns and ps range. Pump–probe TEM (FIG. 2b4) has therefore been used to directly visualize the motion of nanostructured materials, which has direct relevance for the miniaturization of mechanical devices[,257-264]. Examples include the probing of the resonance response of nanoscale cantilever samples[257-259], the determination of the anisotropic bond stiffness and Young's modulus of small protein amyloid fibers associated with Alzheimer's disease[,260,261], and the visualization of strain release dynamics in photoexcited 2D materials[262]. In the latter study, the authors recorded a ns-resolved movie of thermal-stress-induced bulging and buckling of a suspended black phosphorous membrane after laser excitation. They used dark-field imaging, *i.e.*, the selection of specific diffraction peaks, to relate the Bragg-scattering diffraction efficiency to the orientation of local lattice planes (FIG. 6a). The strain in the films was relaxed with different rates along orthogonal crystal directions, an effect that originates from the strongly anisotropic pleated

honeycomb structure of black phosphorous. Strain fields in 2D materials are known to modulate electrical and optical properties[265], thereby providing means to tailor fast spatiotemporal responses to light with important applications in sensors, actuators, and tunable (opto)electronic transducers.

The study of the dynamics of confined fluids within nanoscale structures (nanofluidics), or the dynamics of nanoparticles in liquids, is an emerging field in nanoscience. For example, researchers found that water flows with almost no friction through carbon nanotubes, and that it paradoxically flows faster in narrower tubes, confounding long-standing theories of fluid dynamics[266]. Furthermore, the motion (rotation and translation) of nanometer-sized particles in liquids are dominated by surface effects and may substantially differ from objects of micrometer dimensions and above[251,267]. Time-resolved TEM allows these dynamics to be directly imaged on the nanometer scale, and thereby enables correlation of the nanostructure morphology with fluid transport properties. For example, pump–probe TEM with ns resolution has been used to visualize the flow of liquid lead inside ZnO nanotubes[141]. The lead was molten by applying short heating laser pulses after which the irreversible dynamics was probed using single-shot electron pulses (FIG. 2b2). The reversible heating and cooling rates of the nanotubes were determined stroboscopically (FIG. 2b3). The role of viscous friction on the nanoscale, as well as mechanical properties, such as the slip length, were elucidated by recording the expansion dynamics of the lead column as a function of time delay (FIG. 6b). Pump–probe TEM has also been used to study the morphological dynamics of Au nanodroplets on a graphene surface[100] and the rotational dynamics of Au nanoparticles in aqueous solution[140]. On the other hand, time-resolved TEM under a constant perturbation has been used (FIG. 2a), for example, for studying the self-assembly of nanoparticles in liquids[268-271], bubble nucleation and migration in core–shell nanoparticles[238], and rotation and translation of anisotropic nanoparticles adsorbed at a liquid–solid interface[272], on the

time scale of (milli)seconds. Time-resolved TEM may also prove useful for the investigation of bubble-propelled catalytic nanomotors[273,274], a topic that has received significant attention for applications such as drug delivery, sensing, nanorobotics, and water remediation[275].

Conclusions and outlook

In this Review, we summarized state-of-the-art techniques for time-resolved TEM and their recent application to the study of chemical dynamics of nanoscale materials. We have highlighted the breath of timescales that are covered, from femtoseconds—accessed using pump–probe schemes, to milliseconds/hours—achieved by the use of (fast) cameras. Concurrent developments in TEM holders now allow for a large variety of triggers to be applied and the real conditions inside batteries, catalysts, or devices to be replicated. At the same time, sophisticated data processing and analysis tools have been developed for extracting relevant information from such complex experiments. These advances have transformed TEM from a static *post mortem* characterization tool for materials science of hard materials, to a dynamic *in situ* and *in operando* tool for chemistry of complex, functional materials.

Owing to the phenomenal improvements in spatial and energy resolutions[276,277,278], temporal resolution may be the last dimensional frontier in TEM. For addressing the many challenges that remain, the time domain in TEM ought to receive the same level of investment and attention that the space domain has received[277,278], and that the energy domain[67,71,72,279] is currently receiving, in order to address the myriad of challenges that remain. FIG. 7 highlights some of the key goals, enabling technologies, and "dream" experiments that drive the future development of time-resolved *in situ* TEM[276,280]. Among the goals are the simultaneous increase of the spatial and temporal resolutions to reach respectively the Ångstrom and attosecond (as) regimes[281-284], while

concurrently increasing the complexity of the sample environment. While high-source brightness may be desirable for pump–probe experiments, which require atomic-scale resolution, for materials dynamics at lower resolution one is often willing to sacrifice source brightness for increased counts. Such experiments require sources and instrument configurations that provide high beam currents at low repetition rates while also preserving sub-ps time and sub-nm spatial resolutions. Clearly, there is a need for highly versatile instruments that allow users to deliberately manipulate beam properties—such as pulse duration, intensity, frequency, and coherence—depending on the desired application. This can be achieved through an ingenious combination of laser and electron gun technologies, energy filters, beam deflectors, RF cavities, apertures, detectors, and data acquisition and processing schemes. More systematic experimental and theoretical explorations of the impact of these technologies on beam properties are needed to leverage them to their full capacity.

The control of beam properties may prove to be especially important in the mitigation of electron beam induced effects, which is a ubiquitous challenge in *in situ* TEM experiments. Furthermore, the emerging use of RF cavities make pump–probe TEM a more accessible technique by removing the need for pulsed lasers to generate short pulses of electrons. The synchronization of electron pulse arrival or fast detector readout with the application of cyclic stimuli on the sample will be particularly important for dose-efficient capturing of short-lived intermediate species. Future electron microscopes based on such technical developments must provide atomic-level details of technologically relevant functionalities, such as transport and reactivity on the relevant timescales, not only in perfect crystals, but also at defects, interfaces, and surfaces. For example, the imaging of catalytic reactions at nanoparticle surfaces requires superb spatial resolution down to the level of an active site and the ability to capture the catalytic event—typically a molecular

rearrangement—with a sufficient temporal resolution. This requires controlled triggering of the reaction, the use of sensitive, fast detectors and/or artificial intelligence to detect such rare events. Pulsed electrons may be used to increase temporal resolution or control electron dose to mitigate damage.

The increasing complexity of future time-resolved TEM instrumentation is expected to yield enormous data sets that exceed existing data processing capabilities. This calls for new approaches to hardware–software integration, the combination with high-performance supercomputing facilities, and the further development of computational approaches based on artificial intelligence. Furthermore, the synergy between *in situ* time-resolved X-ray and electron-based materials characterization techniques offers great potential for detailed elucidation of material structure–property–function relationships across all relevant length and time scales. The integration of future TEM facilities housed in national laboratories with state-of-the-art X-ray tools, such as fourth-generation synchrotrons or X-ray free electron lasers, is thus highly desirable.

References

1. Zugic, B., *et al.* Dynamic restructuring drives catalytic activity on nanoporous gold–silver alloy catalysts. *Nat. Mater.* **16**, 558-564 (2017).
2. Huang, J., *et al.* Potential-induced nanoclustering of metallic catalysts during electrochemical CO_2 reduction. *Nat Commun.* **9**, 3117 (2018).
3. Mitra L. Taheri, *et al.*, Current status and future directions for in situ transmission electron microscopy, *Ultramicroscopy* **170**, 86-95 (2016).
4. Zheng, H., & Zhu, Y. Perspectives on in situ electron microscopy. *Ultramicroscopy*, **180**, 188-196 (2017).
5. Zhang, C., *et al.* Recent progress of in situ transmission electron microscopy for energy materials. *Adv. Mater.* **32**, 1904094 (2020).
6. Jinschek, J. R.; Advances in the environmental transmission electron microscope (ETEM) for nanoscale in situ studies of gas-solid interactions. *Chem. Commun.* 50, 2696-2706 (2014).
7. Su, Z., Baskin, J. S., Zhou, W., Thomas, J. M., & Zewail, A. H. Ultrafast elemental and oxidation-state mapping of hematite by 4D microscopy. *J. Am. Chem. Soc.* **139**, 4916-4922 (2017).
8. Heo, J., Dummett Torres, D., Banerjee, P., & Jain, P. K. In-situ electron microscopy mapping of an order-disorder transition in a superionic conductor. *Nat Commun.* **10,** 1505 (2019).
9. Heo, J., Cho, K., & Jain, P. K. Motion of defections in ion-conducting nanowires. *Nano Letters* **21**, 556-561 (2021).
10. Yu, L., *et al.* Unveiling the microscopic origins of phase transformations: an in situ TEM perspective *Chem. Mater.* **32**, 639-650 (2020).

11. Bergmann, U., *et al.* Using X-ray free-electron lasers for spectroscopy of molecular catalysts and metalloenzymes. *Nat. Rev. Phys.* **3**, 264–282 (2021).
12. Kraus, P.M., Zürch, M., Cushing, S.K., Neumark, D. M., & Leone, S. R. The ultrafast X-ray spectroscopic revolution in chemical dynamics. *Nat. Rev. Chem.* **2**, 82–94 (2018).
13. Chergui, M. time-resolved X-ray spectroscopies of chemical systems: new perspectives. *Struct. Dyn.* **3**, 031001 (2016).
14. Zimmermann, P., *et al*. Modern X-ray spectroscopy: XAS and XES in the laboratory *Coord. Chem. Rev.* **423**, 213466 (2020).
15. Smith J.G., Chakraborty I., & Jain P.K.. In situ single-nanoparticle spectroscopy study of bimetallic nanostructure formation. *Angew. Chem. Int. Ed. Engl.* **55**, 9979-9983 (2016).
16. van der Veen, R. M., Kwon, O.-H., Tissot, A., Hauser, A., & Zewail, A. H. Single-nanoparticle phase transitions visualized by four-dimensional electron microscopy. *Nat. Chem.* **5,** 395–402 (2013).
17. van der Veen, R. M., Tissot, A., Hauser, A., & Zewail, A. H. Unusual molecular material formed through irreversible transformation and revealed by 4D electron microscopy. **Phys. Chem. Chem. Phys. 15**, 7831-7838 (2013).
18. Arbouet, A., Caruso, G. M., & Houdellier, F. Chapter one - Ultrafast transmission electron microscopy: historical development, instrumentation, and applications. *Adv. Imaging Electron Phys.*, **207**, 1-72 (2018).
19. Montgomery, E., Leonhardt, D., & Roehling, J. Ultrafast transmission electron microscopy: techniques and applications. *Microscopy Today*, **29**, 46-54 (2021).
20. Vanacore, G.M., Fitzpatrick, A.W.P., & Zewail, A.H., Four-dimensional electron microscopy: Ultrafast imaging, diffraction and spectroscopy in materials science and biology, *Nano Today*, **11**, 228-249 (2016).
21. Adhikari, A., *et al.* Four-dimensional ultrafast electron microscopy: insights into an emerging technology. *ACS Appl. Mater. Interfaces*, **9**, 3-16 (2017)**.**
22. Zewail, A. H. Four-Dimensional Electron Microscopy, *Science*, **328**, 187-193 (2010).
23. Siwick, B. J., Arslan, I, & Wang, X. Frontier nonequilibrium materials science enabled by ultrafast electron methods *MRS Bull.* **46**, 688-693 (2021)
24. Kashin, A.S., & Ananikov, V.P. Monitoring chemical reactions in liquid media using electron microscopy. *Nat. Rev. Chem.* **3,** 624–637 (2019).
25. Ophus, C. Four-dimensional scanning transmission electron microscopy (4D-STEM): from scanning nanodiffraction to ptychography and beyond. *Micros. Microanal*, **25**, 563-582 (2019).
26. Boyes, E. D., LaGrow, A. P., Ward, M. R., Martin, T. E., & Gai, P. L. Visualizing single atom dynamics in heterogeneous catalysis using analytical in situ environmental scanning transmission electron microscopy. *Phil Trans. R. Soc. A.* **378**, 20190605 (2020).
27. Gai, P. L., Sharma, R., & Ross, F. M. Environmental (S)TEM studies of gas–liquid–solid interactions under reaction conditions. *MRS Bull.* **33**, 107-114 (2008).
28. Egerton, R.F., Li, P., & Malac, M., Radiation damage in the TEM and SEM. *Micron*. **35**, 399-409 (2004).
29. Wu, S., *et al*. Evolution of oxyhalide crystals under electron beam irradiation: an in situ method to understand the origin of structural instability. *Inorg. Chem.* **57**, 8988-8993 (2018).
30. de Jonge, N., Peckys, D. B., Kremers, G. J., & Piston, D. W.. Electron microscopy of whole cells in liquid with nanometer resolution. *Proc. Natl. Acad. Sci. USA* **106**, 2159-2164 (2009).
31. Niu, K.-Y., Liao, H.-G., & Zheng, H. Revealing dynamic processes of materials in liquids using liquid cell transmission electron microscopy. *J. Vis. Exp.* **70**, 50122 (2012).
32. Yuk, J. M., *et al.* High-resolution EM of colloidal nanocrystal growth using graphene liquid cells. *Science*, **336**, 61-64 (2012).
33. Kim, B. H., *et al*. Critical differences in 3D atomic structure of individual ligand-protected nanocrystals in solution. *Science*, **368**, 60-67 (2020).
34. Hauwiller, M. R., Ondry, J. c., & Alivisatos, A. P. Using graphene liquid cell transmission electron microscopy to study *in situ* nanocrystal etching. *J. Vis. Exp.* **135**, e57665 (2018).
35. Mele, L*, et al.* A MEMS-based heating holder for the direct imaging of simultaneous *in-situ* heating and biasing experiments in scanning/transmission electron microscopes. *Microsc. Res. Tech.* **79**, 239-250 (2016).
36. Allard, L.F., *et al.* A new MEMS-based system for ultra-high-resolution imaging at elevated temperatures. *Microsc. Res. Tech.*, **72**, 208-215 (2009).
37. Shindo, D., *et al.* Development of a multifunctional TEM specimen holder equipped with a piezodriving probe and a laser irradiation port, *J. Electron Microsc. (Tokyo)*, **58**, 245–249 (2009).
38. Zhang, C., *et al.* D. Statistically analyzed photoresponse of elastically bent CdS nanowires probed by light-compatible in situ high-resolution TEM. *Nano Lett.* **16**, 6008-6013 (2016).

39. Vadai, M., Angell, D.K., Hayee, F., Sytwu, K., & Dionne, J. A. In-situ observation of plasmon-controlled photocatalytic dehydrogenation of individual palladium nanoparticles. *Nat. Commun.* **9,** 4658 (2018).
40. Zhang, L., Miller, B. K., & Crozier, P. A. Atomic level in situ observation of surface amorphization in anatase nanocrystals during light irradiation in water vapor. *Nano Lett.* **13**, 679-684 (2013).
41. Goncalves, F.J.T., *et al.* Probing microwave fields and enabling in-situ experiments in a transmission electron microscope. *Sci. Rep.* **7**, 11064 (2017).
42. Weßels, T., *et al*. Continuous illumination picosecond imaging using a delay line detector in a transmission electron microscope, *Ultramicroscopy*, **233**, 113392 (2022).
43. Fu, X., *et al*. Direct visualization of electromagnetic wave dynamics by laser-free ultrafast electron microscopy. *Science Adv.* **6**, eabc3456 (2020).
44. Dong, H., *et al.* Simultaneous atomic-level visualization and high precision photocurrent measurements on photoelectric devices by in situ TEM. **RSC Adv. 8**, 948-953 (2018).
45. Picher, M., Maxxucco, S., Blankenship, S., & Sharma, R.. Vibrational and optical spectroscopies integrated with environmental transmission electron microscopy. *Ultramicroscopy*, **150**, 10-15 (2015).
46. Houdellier, F., Caruso, G. M., Weber, S., Kociak, M., & Arbouet, A. Development of a high brightness ultrafast Transmission Electron Microscope based on a laser-driven cold field emission source, *Ultramicroscopy*, **186**, 128-138 (2018).
47. Kim, Y.-J., & Kwon, O.-H. Cathodoluminesence in ultrafast electron microscopy. *ACS Nano*, **15**, 19480-19489 (2021).
48. J Huang, J. Y., *et al.* In Situ observation of the electrochemical lithiation of a single SnO2 nanowire electrode. *Science*, **330**, 1515-1520 (2010).
49. Li, X., Turner, J., Bustillo, K., & Minor, A. M. In situ transmission electron microscopy investigation of electroplasticity in single crystal nickel. *Acta Mater.*, **223**, 117461 (2022).
50. Plodinec, M., Nerl, H. C., Girgsdies, F., Schlögl, R., Lunkenbein, T. Insights into chemical dynamics and their impact on the reactivity of Pt nanoparticles during CO oxidation by operando TEM. *ACS Catal.* **2020**, *10* (5), 3183-3193. DOI: 10.1021/acscatal.9b03692
51. Jiang, Y., Li, H., Wu, Z., Ye, W., Zhang, H., Wang, Y., Sun, C., Zhang, Z. In situ observation of hydrogen-induced surface faceting for palladiaum-copper nanocrystals at atmospheric pressure. *Angew. Chem. Int. Ed.* **55**, 12427-12430 (2016).
52. Gao, W., *et al.* Dynamics of transformation from platinum icosahedral nanoparticles to larger FCC crystal at millisecond time resolution. *Sci. Rep.* **7,** 17243 (2017).
53. Vendelbo, S. B., *et al*. Visualization of oscillatory behaviour of Pt nanoparticles catalysing CO oxidation. *Nature Mater.* **13**, 884–890 (2014).
54. Yoshida, H., *et al.* Visualizing gas molecules interacting with supported nanoparticulate catalysts at reaction conditions, *Science*, **335**, 317-319 (2012).
55. Levin, B. D. A., Direct detectors and their applications in electron microscopy for materials science. *J Phys. Mater.*, **2021**, *4*, 042005.
56. Kuhlbrandt, W.. The Resolution Revolution. *Science*, **343**, 1443-1444 (2014).
57. Nakane, T. *et al.* Single-particle cryo-EM at atomic resolution. **587**, 152-156 (2020).
58. Plotkin-Swing, B., *et*. al. Hybrid pixel direct detector for electron energy loss spectroscopy. *Ultramicroscopy*, **217**, 113067 (2020).
59. Beacham, R., *et al*. Medipix2/Timepix detector for time resolved Transmission Electron Microscopy. *J. Instrum.*, **6**, C12052 (2011).
60. Ryll, H., *et al*. A pnCCD-based, fast direct single electron imaging camera for TEM and STEM. *J. Instrum.*, **11**, P04006 (2016)
61. McMullan, G., Faruqi, A. R., Clare, D., & Henderson, R. Comparison of optimal performance at 300 keV of three direct electron detectors for use in low dose electron microscopy, *Ultramicroscopy*, **147**, 156-163 (2014).
62. Faruqi, A. R., Henderson, R., Pryddetch, M., Allport, P., & Evans, A. Direct single electron detection with a CMOS detector for electron microscopy. *Nuc Inst.* **546**, 170-175 (2005).
63. McMullan, G., Chen, S., Henderson, R., & Faruqi, A. R. Detective quantum efficiency of electron area detectors in electron microscopy. *Ultramicroscopy*, **109**, *109*, 1126-1143 (2009).
64. Ercius, P., *et al.* The 4D camera – An 87 kHz frame-rate detector for counted 4D-STEM experiments. *Microsc. Microanal.* **26**, 1896-1897 (2020).
65. van der Veen, R. M., Penfold, T. J., & Zewail, A. H. Ultrafast core-loss spectroscopy in four-dimensional electron microscopy. *Struct. Dyn.* **2**, 024302 (2015).

66. Carbone, F., Kwon, O., & Zewail, A. H. Dynamics of chemical bonding mapped by energy-resolved 4D electron microscopy. *Science*, **325**, 181-184 (2009).
67. Krivanek, O. L., *et al.* Vibrational spectroscopy in the electron microscope. *Nature* **514**, 209–212 (2014).
68. Nomura, Y., *et al.* Dynamic imaging of lithium in solid-state batteries by *operando* electron energy-loss spectroscopy with sparse coding. *Nat. Commun.* **11,** 2824 (2020).
69. Pomarico, E., *et al*. Ultrafast electron energy-loss spectroscopy in transmission electron microscopy. *MRS Bull.* **43**, 497–503 (2018).
70. Vanacore, G. M., van der Veen, R. M., & Zewail, A. H. Origin of axial and radial expansions in carbon nanotubes revealed by ultrafast diffraction and spectroscopy. *ACS Nano*, **9**, 1721-1729 (2015).
71. Pate, C.M., Hart, J.L., & Taheri, M.L. RapidEELS: machine learning for denoising and classification in rapid acquisition electron energy loss spectroscopy. *Sci. Rep.* **11**, 19515 (2021).
72. Hart, J.L., *et al.* Direct detection electron energy-loss spectroscopy: a method to push the limits of resolution and sensitivity. *Sci. Rep.* **7**, 8243 (2017).
73. Verhoeven, W., *et al*. Design and characterization of dielectric filled TM110 microwave cavities for ultrafast electron microscopy. *Rev. Sci. Instrum.* **90**, 083703 (2019).
74. Qiu, J., *et al.* GHz laser-free time-resolved transmission electron microscopy: A stroboscopic high-duty-cycle method. *Ultramicroscopy*, **161**, 130-136 (2016).
75. Jannis, D., Müller-Caspary, K., Beche, A., Oelsner, A., & Verbeeck. Spectroscopic coincidence experiments in transmission electron microscopy. *Appl. Phys. Lett.* **114**, 143101 (2019).
76. Campbell, M., *et. al.* Towards a new generation of pixel detector readout chips. *J. Instum.* **11**, C01007 (2016).
77. He, Y., Lie, J.-C., Luo, L., & Wang, C. Size Dependent dynamic structures of supported gold nanoparticles in CO oxidation reaction conditions. *Proc. Natl. Acad. Sci. USA*, **115**, 7700-7705 (2018).
78. Yuan, W., *et al.* In situ manipulation of the active Au-TiO2 interface with atomic precision during CO oxidation. *Science*, **371**, 517-521 (2021).
79. Datta, A., *et al.* A data reduction and compression description for high throughput time-resolved electron microscopy. *Nat. Commun.* **12,** 664 (2021).
80. Horwath, J.P., Zakharov, D.N., Mégret, R., & Stach, E. A. Understanding important features of deep learning models for segmentation of high-resolution transmission electron microscopy images. *npj Comput. Mater.* **6**, 108 (2020).
81. Stevens, A., *et al.* Applying compressive sensing to TEM video: a substantial frame rate increase on any camera. *Adv. Struct. Chem. Imag.* **1**, 10 (2015).
82. Reed, B. W., *et al.* Electrostatic subframing and compressive-sensing video in transmission electron microscopy. *Struct. Dyn.* **6**, 054303 (2019).
83. Liu, X., Zhang, S., Yurtsever, A., & Liang, J. Single-shot real-time sub-nanosecond electron imaging aided by compressed sensing: Analytical modeling and simulation. *Micron*, **117**, 47-54 (2019).
84. Zandi, O., *et al.* Transient lensing from a photoemitted electron gas imaged by ultrafast electron microscopy. *Nat. Commun.* **11**, 3001 (2020).
85. Lau, J. W., *et al.* Laser-free GHz stroboscopic transmission electron microscope: Components, system integration, and practical considerations for pump-probe measurements. *Rev. Sci. Instrum.* **91**, 021301 (2020).
86. Nukala, P., *et al.* Inverting polar domains via electrical pulsing in metallic germanium telluride. *Nat. Commun.* **8**, 15033 (2017).
87. Voisin, T., *et al.* In Situ TEM observations of high-strain-rate deformation and fracture in pure copper. *Materials Today*, **33**, 10-16 (2020).
88. Sohn, S., Xie, Y., Jung, Y. Schroers, J., & Cha, J. J. Tailoring crystallization phases in metallic glass nanorods via nucleus starvation. *Nat. Commun.* **8**, 1980 (2017).
89. Orava, J., *et al.* In situ correlation between metastable phase-transformation mechanism and kinetics in a metallic glass. *Nat. Commun.* **12**, 2839 (2021).
90. Kim, J. S., *et al.* Imaging of transient structures using nanosecond in situ TEM. *Science*, **321**, 1472-1475 (2008).
91. Olshin, P. K., Bongiovanni, G., Drabbels, M., & Lorenz, U. J. Atomic-resolution imaging of fast nanoscale dynamics with bright microsecond electron pulses. *Nano Lett.* **21**, 612-618 (2021).
92. Zhang, L., Hoogenboom, J. P., & Kruit, P., Photoemission sources and beam blankers for ultrafast electron microscopy. *Struct. Dyn.* **6**, 051501 (2019).
93. LaGrange, T., *et al.* Nanosecond time-resolved investigations using the in situ of dynamic transmission electron microscopy (DTEM). *Ultramicroscopy*, **108**, 1441-1449 (2008).

94. Piazza, L., *et al*. Design and implementation of a fs-resolved transmission electron microscope based on thermionic gun technology. *Chemical Physics*, **423**, 79-84 (2013).
95. Bucker, K., *et al.* Electron beam dynamics in an ultrafast transmission electron microscope with Wehnelt electrode. *Ultramicroscopy*, **171**, 8-18 (2016).
96. Lee, Y. M., Kim, Y. J., Kim, Y.-J., & Kwon, O.-H. Ultrafast electron microscopy integrated with a direct electron detection camera. *Struct. Dyn.* **4**, 044023 (2017).
97. Plemmons, D. A., & Flannigan, D. J., Ultrafast electron microscopy: instrument response from the single-electron to high bunch-charge regimes. *Chem. Phys. Lett.*, **683**, 186-192 (2017).
98. Ji, S., *et al.* Influence of cathode geometry on electron dynamics in an ultrafast electron microscope, *Struct. Dyn*. **4**, 054303 (2017).
99. Feist, A., *et al*. Ultrafast transmission electron microscopy using a laser-driven field emitter: Femtosecond resolution with a coherence electron beam. *Ultramicroscopy* **176**, 63-73 (2017).
100. Olshin, P. K., Drabbels, M., & Lorenz, U. J. Characterization of a time-resolved electron microscope with a Schottky field emission gun. *Struct. Dyn*. **7**, 054304 (2020).
101. Zhu, C. Et al. Development of analytical ultrafast transmission electron microscopy based on laser-driven Schottky field emission. *Ultramicroscopy*, **209**, 112887 (2020).
102. Sinha, S.K. *et al.* Nanosecond electron pulses in the analytical electron microscopy of a fast irreversible chemical reaction. *Nat. Commun.* **10**, 3648 (2019).
103. Denham, P., & Musumeci, P. Space-charge aberrations in single-shot time-resolved transmission electron microscopy. *Phys. Rev. Applied*, **15**, 024050 (2021).
104. Berger, J. A., *et. al.* DC photoelectron gun parameters for ultrafast electron microscopy. *Microsc. Microanal.* **15**, 298-313 (2009).
105. Picher, M., Bucker, K., LaGrange, T., & Banhart, F. Imaging and electron energy-loss spectroscopy using single nanosecond electron pulses. *Ultramicroscopy*, **188**, 41-47 (2018).
106. Reed, B.W., *et al*. Solving the accelerator-condenser coupling problem in a nanosecond dynamic transmission electron microscope. *Rev. Sci. Instrum*. **81**, 053706 (2010).
107. Ji, F., *et al.* Ultrafast relativistic electron nanoprobes. *Commun. Phys.* **2**, 54 (2019).
108. Yang, J., & Yoshida, Y. Relativistic ultrafast electron microscopy: single-shot diffraction imaging with femtosecond electron pulses, *Adv. Condens. Matter Phys.* **2019**, 9739241 (2019).
109. Yang, J., Yoshida, Y., & Yasuda, H. Ultrafast electron microscopy with relativistic femtosecond electron pulses. *Microscopy*, **67**, 291–295 (2018).
110. Li, R. K., & Musumeci, P. Single-Shot MeV Transmission electron microscopy with picosecond temporal resolution. *Phys Rev Appl.* **2**, 024003 (2014).
111. Xiang, D. *et al.*, Accelerator-based single-shot ultrafast transmission electron microscope with picosecond temporal resolution and nanometer spatial resolution. *Nuc. Instrum*. **759**, 74-82 (2014).
112. Wan, W., Chen, F.-R., & Zhu, Y. Design of compact ultrafast microscopes for single- and multi-shot imaging with MeV electrons. *Ultramicroscopy*, **194**, 143-153 (2018).
113. Musumeci, P., Moody, J. T., & Scoby, C. M. Relativistic electron diffraction at the UCLA Pegasus photoinjector laboratory. *Ultramicroscopy*, **108**, 1450-1453 (2008).
114. van Oudheusden, T., *et al.* Compression of subrelativistic space-charge-dominated electron bunches for single-shot femtosecond electron diffraction. *Phys. Rev. Lett.* **105**, 264801 (2010).
115. Weathersby, S. P., *et al*. Mega-electron-volt ultrafast electron diffraction at SLAC National Accelerator Laboratory *Rev. Sci. Instrum*. **86**, 073702 (2015).
116. Manz, S. *et al.* Mapping atomic motions with ultrabright electrons: towards fundamental limits in space-time resolution. *Faraday Discuss.* **177**, 467-491 (2015).
117. Wu, J., Tang, M., Zhao, L., & Zhang, J. Ultrafast atomic view of laser-induced melting and breathing motion of metallic liquid clusters with MeV ultrafast electron diffraction. *Proc. Natl. Acad. Sci. USA.* **119**, e2111949119 (2022).
118. Domer, H., & Bostanjoglo, O. High-speed transmission electron microscope. *Rev. Sci. Inst.* **74**, 4369 (2003).
119. LaGrange, T., Reed, B. W., & Masiel, D. J. Movie-mode dynamic electron microscopy. *MRS Bull.* **40**, 22-28 (2105).
120. Roehling, J. D., *et al.* Rapid solidification growth mode transitions in Al-Si alloys by dynamic transmission electron microscopy. *Acta Mater*. **131**, 22-30 (2017).
121. Egan, G. C., LaGrange, T., & Zachariah, M. R. Time-resolved imaging of nanoscale condensed phase reaction. *J. Phys. Chem. C.* **119**, 2792-2797 (2015).

122. Santala, M. K., *et al.* Irreversible reactions studied with nanosecond transmission electron microscopy movies: Laser crystallization of phase change materials. *Appl. Phys. Lett.* **102**, 174105 (2013).
123. Yoo, B.-K., Kwon, O.-H., Liu, H., Tang, J., & Zewail, A. H. Observing in space and time the ephemeral nucleation of liquid-to-crystal phase transitions. *Nat. Commun.* **6**, 8639 (2015).
124. Reisbick, S. A. *et. al.* Stroboscopic ultrafast imaging using RF strip-lines in a commercial transmission electron microscope. *Ultramicroscopy*, **235**, 113497 (2022).
125. Barwick, B., Park, H. s., Kwon, O.-H., Baskin, J. S., & Zewail, A. H. 4D imaging of transient structures and morphologies in ultrafast electron microscopy. *Science*, **322**, 1227-1231 (2008).
126. Cao, G. *et al.* Clocking the anisotropic lattice dynamics of multi-walled carbon nanotubes by four-dimensional ultrafast transmission electron microscopy. *Sci. Rep.* **5**, 8404 (2015).
127. Valley, D. T., Ferry, V. E., & Flannigan, D. J. Imaging intra- and interparticle acousto-plasmonic vibrational dynamics with ultrafast electron microscopy. *Nano Lett.* **16**, 7302-7308 (2016).
128. Kim, Y.-J., Jung, H., Han, S. W., & Kwon, O.-H.; Ultrafast electron microscopy visualizes acoustic vibrations of plasmonic nanorods at the interfaces. *Matter*, **1**, 481-495 (2019).
129. Otto, M. R., Rene de Cotret, L. P., Stern, M. J., Siwick, B. J. Solving the jitter problem in microwave compressed ultrafast electron diffraction instruments: Robust sub-50 fs cavity-laser phase stabilization. *Struct. Dyn.* **4**, 051101 (2017).
130. Snively, E. C., *et al.* Femtosecond compression dynamics and timing jitter suppression in a THz-driven electron bunch compressor. *Phys. Rev. Lett*, **124**, 054801 (2020).
131. Kealhofer, C., *et al.* All-optical control and metrology of electron pulses. *Science*, **352**, 429-433 (2016).
132. Williams, J., *et al*.. Active control of bright electron beams with RF optics for femtosecond microscopy. *Struct. Dyn.* **4,** 044035 (2017).
133. Rozenzweig, J. B., *et al.* Next generation high brightness electron beams from ultrahigh field cryogenic rf photocathode sources. *Phys. Rev. Accel. Beams*, **22**, 023403 (2019).
134. Hassan, M. T., Liu, H., Basking, J. S., Zewail, A. H. Photon gating in four-dimensional ultrafast electron micrscopy. *Proc, Nat. Acad. Sci. USA*, **112**, 12944-12949 (2015).
135. Fu, X., *et al.* Nanoscale-femtosecond dielectric response of Mott insulators captured by two-color near-field ultrafast electron microscopy. *Nat. Commun.* **11**, 5770 (2020).
136. Liu, H., Kwon, O-H., Tang, J., & Zewail, A. H. 4D imaging and diffraction dynamics of single-particle phase transition in heterogeneous ensembles. *Nano Lett.* **14**, 946-954 (2014).
137. Voss J. M., Harder, O. F., Olshin, P. K., Drabbels, M, & Lorenz, U. J. Rapid melting and revitrification as an approach to microsecond time-resolved cryo-electron microscopy. *Chem. Phys. Lett.* **778**, 138812 (2021).
138. Danz, T., Domrose, T., & Ropers, C. Ultrafast nanoimaging of the order parameter in a structural phase transition. *Science*, **371**, 371-374 (2021).
139. Fu, X., Chen, B., Tang, J., & Zewail, A. H. Photoinduced nanobubble-driven superfast diffusion of nanoparticles imaged by 4D electron microscopy. *Sci. Adv.* **3**, e1701160 (2017).
140. Fu, X., Chen, B., Tang, J., Hassan, M. T., & Zewail, A. H.. Imaging rotational dynamics of nanoparticles in liquid by 4D electron microscopy. *Science*. **355**, 494-498 (2017).
141. Lorenz, U. J., & Zewail, A. H. Observing liquid flow in nanotubes by 4D electron microscopy. *Science*. **344**, 1496-1500 (2014).
142. Barwick, B., Flannigan, D. H., & Zewail, A., H. Photon-induced near-field electron microscopy. *Nature.* **462**, 902–906 (2009).
143. Liu, H., *et al.* Visualization of plasmonic couplings using ultrafast electron microscopy. *Nano Lett*. **21,** 5842-5849 (2021).
144. Yurtsever, A., van der Veen, R. M., & Zewail, A. H. Subparticle ultrafast spectrum imaging in 4D electron microscopy. *Science*, **335**, 59-64 (2012).
145. Kaplan, M. et. al. Photon-induced near-field electron microscopy of eukaryotic cells. *Angew. Chem. Int. Ed.* **56**, 11498-11501 (2017).
146. Pomarico, E., *et al.* meV resolution in laser-assisted energy filtered transmission electron microscopy. *ACS Photonics* **5**, 759-764 (2018).
147. Kurman, T., *et al.* Spatiotemporal imaging of 2D Polariton wave packet dynamics using free electrons. *Science*, **372**, 1181-1186 (2021).
148. Sun, S., *et al.* Direct imaging of plasma waves using ultrafast electron microscopy. *Struct. Dyn.* **7**, 064301 (2020).
149. Spivak, G. V., Dyukov, V. G., Sedov, N. N., & Nevzorov A. N. A stroboscopic secondary-emission electron microscope. *Bull. Acad. Sci. USSR, Phys. Ser*. **30,** 769-775 (1966).

150. Bostanjoglo, O., & Rosin, T. Ultrasonically induced magnetic reversals observed by stroboscopic electron microscopy. *Int. J. Opt.* **24**, 657-664 (1977).
151. Plows, G. S., & Nixon, W. C. Stroboscopic scanning electron microscopy. *J. Phys. E: Sci. Instrum.* **1**, 595-600 (1968).
152. Ura, K., Fujioka, H., Hosokawa, T. Picosecond pulse stroboscopic scanning electron microscope. *J. Electron. Microsc.* **27**, 247-252 (1978).
153. Jing, C., *et al.* Tunable electron beam pulser for picoseconds stroboscopic microscopy in transmission electron microscopes. *Ultramicroscopy*, **207**, 112829 (2019).
154. Weppelman, I. G. C., Moerland, R. J., Hoogenboom, J. P., & Kruit, P. Concept and design of a beam blanker with integrated photoconductive switch for ultrafast electron microscopy. *Ultramicroscopy*, **184**, 8-17 (2018).
155. Lassise, A., Mutsaers, P. H. A., & Luiten, O. J., Compact, low power radio frequency cavity for femtosecond electron microscopy. *Rev. Sci. Instrum.* **83**, 043705 (2012).
156. VandenBussche. E. J., & Flannigan, D. J. Reducing radiation damage in soft matter with femtosecond-timed single-electron packets. *Nano Lett.* **19**, 6687-6694 (2019).
157. VandenBussche, E. J., Clark, C. P., Holmes, R. J., & Flannigan, D. J. Mitigating Damage to Hybrid Perovskites Using Pulsed-Beam TEM. *ACS Omega*. **5**, 31867-31871 (2020).
158. Kisielowski, C., *et al.* Discovering hidden material properties of $MgCl_2$ at atomic resolution with structured temporal electron illumination of picosecond time resolution. *Adv. Funct. Mater.* **29**, 1807818 (2019).
159. Mariette, C., *et al.* Strain wave pathway to semiconductor-to-metal transition revealed by time-resolved X-ray powder diffraction. *Nat. Commun.* **12**, 1239 (2021).
160. Bertoni, R., *et al.* Elastically driven cooperative response of a molecular material impacted by a laser pulse. *Nat. Mater.* **15**, 606–610 (2016).
161. Paterson, G. W., *et al.* Sub-100 nanosecond temporally resolved imaging with the medipix3 direct electron detector. *Ultramicroscopy*, **210**, 112917 (2020)
162. Ali, H. *et al.* An electron energy loss spectrometer based streak camera for time resolved TEM measurements. *Ultramicroscopy*, **176**, 112917 (2017).
163. Verhoeven, W., *et al.* Time-of-flight electron energy loss spectroscopy by longitudinal phase space manipulation with microwave cavities. *Struct. Dyn.* **5**, 051101 (2018).
164. Bloom, R, Park, S. T., Reed, B., & Masiel, D. High framerate and high dynamic range electron microscopy. https://patents.justia.com/patent/20210082661 (2020).
165. Yuan, W., *et al.* Visualizing H_2O molecules reacting at TiO_2 active sites with transmission electron microscopy. *Science*, **367**, 428-430 (2020).
166. Yang, J., *et al.* Formation of two-dimensional transition metal oxide nanosheets with nanoparticles as intermediates. *Nat. Mater.* **18,** 970–976 (2019).
167. Sytwu, K., *et al.* Driving energetically unfavorable dehydrogenation dynamics with plasmonics. *Science*, **371**, 280-283 (2021).
168. Bai, S., Gao, C., Low, J, & Xiong, Y. Crystal phase engineering on photocatalytic materials for energy and environmental applications. *Nano Res.* **12**, 2031–2054 (2019).
169. Gavhane, D.S., *et al.* In situ electron microscopy study of structural transformations in 2D $CoSe_2$. *npj 2D Mater. Appl.* **5**, 24 (2021).
170. Li, J., Wang, Z., & Deepak, F. L. Direct atomic-scale observation of intermediate pathways of melting and crystallization in supported Bi nanoparticles. *J. Phys. Chem. Lett.* **9**, 961-969 (2018).
171. Zou, L., Li, J., Zakharov, D., Stach, E. A., & Zhou, G. In situ atomic-scale imaging of the metal/oxide interfacial transformation. *Nat. Commun.* **8**, 307 (2017).
172. Ghosh, C., *et al.* Phase evolution and structural modulation during in situ lithiation of MoS_2, WS_2 and graphite in TEM. *Sci. Rep.* **11**, 9014 (2021).
173. McDowell, M. T., *et al.* In situ observation of divergent phase transformations in individual sulfide nanocrystals. *Nano Lett.* **15**, 1264-1271 (2015).
174. Ross, F. M. Opportunities and challenges in liquid cell electron microscopy. *Science*, **350**, 1490 (2015).
175. Sarkar, R., Rentenberger, C., & Rajagopalan, J. Electron Beam Induced Artifacts During *in situ* TEM Deformation of Nanostructured Metals. *Sci. Rep.* **5**, 16345 (2015).
176. Yao, L., *et al.* Electron-beam-induced perovskite–Brownmillerite–perovskite structural phase transitions in epitaxial $La_{2/3}Sr_{1/3}MnO_3$ films. *Adv. Mater.*, **26,** 2789-2793 (2014).
177. Han, S., *et al.* Gas-assisted transformation of gold from fcc to the metastable 4H phase. *Nat. Commun.* **11**, 552 (2020).

178. Funk, H., *et al.* In situ TEM monitoring of phase-segregation in inorganic mixed halide perovskite. *J. Phys. Chem. Let* **11**, 4945-4950 (2020).
179. Nakamuro, T., Sakakibara, M., Nada, H., Harano, K., & Nakamura, E. Capturing the moment of emergence of crystal nucleus from disorder. *J. Am. Chem. Soc.* **143,** 1763-1767 (2021).
180. Egan, G. C., Sullivan, K. T., LaGrange, T., Reed, B. W., & Zachariah, M. R. In situ imaging of ultra-fast loss of nanostructure in nanoparticle aggregates. *J. Appl. Phys*. **115**, 084903 (2014).
181. Xiang, B., *et al.* situ TEM near-field optical probing of nanoscale silicon crystallization. *Nano Lett.* **12**, 2524-2529 (2012).
182. Park, S. T., Flannigan, D. J., & Zewail, A. H. Irreversible chemical reactions visualized in space and time with 4D electron microscopy. *J. Am. Chem. Soc.* **133**, 1730-1733 (2011).
183. Voss, J. M., Olshin, P. K., Charbonnier, R., Drabbels, M., & Lorenz, U. J. In situ observation of Coulomb fission of individual plasmonic nanoparticles. *ACS Nano* **13**, 12445-12451 (2019).
184. Grapes, M. D., La *et al*. Combining nanocalorimetry and dynamic transmission electron microscopy for in situ characterization of materials processes under rapid heating and cooling. *Rev. Sci. Instrum.* **85**, 084902 (2014).
185. Hada, M., *et al.* Ultrafast time-resolved electron diffraction revealing the nonthermal dynamics of near-UV photoexcitation-induced amorphization in $Ge_2Sb_2Te_5$. *Sci. Rep.* **5,** 13530 (2015)
186. Grinolds, M. S., Lobastov, V. A., Weissenrieder, J., & Zewail, A. H. Four-dimensional ultrafast electron microscopy of phase transitions. *Proc. Natl. Acad. Sci USA*, **103**, 18427-18431 (2006).
187. Park, S. T., & van der Veen, R. M., Modeling nonequilibrium dynamics of phase transitions at the nanoscale: Application to spin-crossover *Struct. Dyn.* **4**, 044028 (2017).
188. Zhang, C., *et al.* Recent progress of in situ transmission electron microscopy for energy materials. *Adv. Mater.* **32**, 1904094 (2020).
189. Liang, J., *et al.* Atomic arrangement engineering of metallic nanocrystals for energy-conversion electrocatalysis. *Joule*, 3, 956-991 (2019).
190. Han, S., *et al.* Interrogation of the reaction mechanism in a Na-O_2 battery using in situ transmission electron microscopy *ACS Nano* **14**, 3669-3677 (2020).
191. Lutz, L., *et al.* Operando monitoring of the solution-mediated discharge and charge processes in a Na-O_2 battery using liquid-electrochemical transmission electron microscopy. *Nano Lett.* **18**, 1280-1289 (2018)
192. Liu, Q., *et al.* In-situ imaging electrocatalysis in a Na-O2 battery with Au-coated MnO2 nanowires air cathode. *En. Stor. Mater.*, **19**, 48-55 (2019).
193. Zhu, Y., *et al.* Probing the electrochemical evolution of Na-CO2 nanobatteries on Pt@NCNT cathodes using in-situ environmental TEM. *En. Stor. Mater*, **33**, 88-94 (2020).
194. Yang, T., *et al.* In situ imaging electrocatalytic CO_2 reduction and evolution reactions in all-solid-state Li-CO_2 nanobatteries. *Nanoscale*, **12**, 23967-23974 (2020).
195. Liu, Q., *et al.* In situ electrochemical study of Na-O_2/CO_2 batteries in an environmental transmission electron microscopy. *ACS Nano* **14**, 13232-13245 (2020).
196. Zhang, W., *et al.* Kinetic pathways of ionic transport in fast-charging lithium titanate. *Science*, **367**, 1030-1034 (2020).
197. Gutiérrez-Kolar, J. S., *et al.* Interpreting electrochemical and chemical sodiation mechanisms and kinetics in tin antimony battery anodes using in situ transmission electron microscopy and computational methods. *ACS Appl. Energy Mater.* **2**, 3578-3586 (2019).
198. Piazza, L., *et al.* Simultaneous observation of the quantization and the interference pattern of a plasmonic near-field. *Nat. Commun.* **6**, 6407 (2015).
199. Cremons, D. R., Plemmons, D. A., & Flannigan, D. J. Femtosecond electron imaging of defect-modulated phonon dynamics. *Nat. Commun.* **7**, 11230 (2016).
200. McKenna, A. J., Eliason, J. K., & Flannigan, D. J. Spatiotemporal evolution of coherent elastic strain waves in a single MoS_2 flake. *Nano Lett.* **17**, 3952-3958 (2017).
201. Zhang, Y., & Flannigan, D. J. Observation of anisotropic strain-wave dynamics and few-layer dephasing in MoS_2 with ultrafast electron microscopy. *Nano Lett.* **19**, 8216-8224 (2019).
202. Gnabasik, R. A., Suri, P. K., Chen, J., & Flannigan, D. J. Imaging coherent phononics and precursor dynamics in LaFeAsO with 4D ultrafast electron microscopy. *Phys. Rev. Mater.* **6**, 024802 (2022).
203. Zhang, Y., & Flannigan, D. J. Imaging nanometer phonon softening at crystal surface steps with 4D ultrafast electron microscopy. *Nano Lett.* **21**, 7332-7338 (2021).
204. Reisbick, S. A., Zhang, Y., Chen, J., Engen, P. E., & Flannigan, D. J. Coherent phonon disruption and lock-in during photoinduced charge-density-wave phase transition. *J. Phys. Chem. Lett.* **12**, 6439-6447 (2021).

205. Reisbick, S. A., Zhang, Y., & Flannigan, D. J. Influence of discrete defects on observed acoustic-phonon dynamics in layered materials probed with ultrafast electron microscopy. *J. Phys. Chem A* **124,** 1877-1884 (2020)
206. Kwak, W.-J., Luo, L., Jung, H.-G., Wang, C., & Sun , Y.-K. revealing the reaction mechanism of Na-O_2 batteries using environmental transmission electron microscopy. *ACS Energy Lett.* **3**, 393-399 (2018).
207. McDowell, M. T., The role of nanoscale science for advancing batteries. *Nano Lett.* **21**, 6353-6355 (2021).
208. Li, Y., & Lu, J. Metal-air batteries: Will they be the future electrochemical energy storage device of choice? *ACS Energy Lett.* **2**, 1370-1377 (2017).
209. Harvey, T. R., *et al.* Probing chirality with inelastic electron-light scattering. *Nano Lett.* **20**, 4377-4383 (2020).
210. Garcia de Abajo, F., J., & Kociak, M. Electron energy-gain spectroscopy. *New. J. Phys.* **10**, 073035 (2008).
211. Konecna, A., Di Giulio, V., Mkhitaryan, V., Ropers, C., & Garcia de Abajo, F., J. Nanoscale nonlinear spectroscopy with electron beams. *ACS Photonics,* **7**, 1290-1296 (2020).
212. Di Giulio, V., Kfir, O., Ropers, C., & Garcia de Abajo, F., J. Modulation of cathodoluminescence emission by interference with external light. *ACS Nano*, **15**, 7290-7304 (2021).
213. Yu, S., Wilson, A. J., Kumari, G., Zhang, X., & Jain, P. K., Opportunities and challenges of solar-energy-driven carbon dioxide to fuel conversion with plasmonic catalysis. *ACS Energy Lett.* **2,** 2058-2070 (2017).
214. Wilson, A. J., Devasia, D., & Jain, P. K. Nanoscale Optical Imaging in Chemistry. *Chem. Soc. Rev.*, **49**, 6087-6112 (2020).
215. Yang, L., Zhou, Z., Song, J., & Chen, X.; Anisotropic nanomaterials for shape-dependent physicochemical and biomedical applications. *Chem. Soc. Rev.* **19**, 5140-5176 (2019).
216. Basov, D. N., Asenjo-Garcia, A., Schuck, P. J., Zhu, X. & Rubio, A. Polariton panorama. *Nanophotonics*. **10**, 549-577 (2021).
217. Ghai, S. S., & Kim, W. T. A novel heat transfer model and its application to information storage systems. *J. Appl. Phys.* **97**, 10P703 (2005).
218. Kandasamy, R., Wang, X.-Q., & Mujumdar, A. S. Application of phase change materials in thermal management of electronics. *Appl. Therm. Eng.* **27**, 2822-2832 (2007).
219. Kumar, L., Hasanuzzaman, M., Rahim, N. A. Global advancement of solar thermal energy technologies for industrial process heat and its future prospects: A review. *Energy Convers. Manag.*, **195**, 885-908 (2019)
220. Park, S. T., Flannigan, D. J., & Zewail, A. H. 4D electron microscopy visualization of anisotropic atomic motions in carbon nanotubes. *J. Am. Chem. Soc.* **134**, 9146-9149 (2012).
221. Hu, J., Vanacore, G. M., Yang, Z., Miao, X., & Zewail, A. H. Transient structures and possible limits of data recording in phase-change materiaks. *ACS Nano* **9**, 6728-6737 (2015).
222. Liu, L., & Corma, A. Structural transformations of solid electrocatalysts and photocatalysts. *Nat Rev Chem* **5**, 256–276 (2021).
223. He, B., Zhang, Y., Liu, X., & Chen, L., In-situ transmission electron microscope techniques for heterogeneous catalysis. *ChemCatChem* **12**, 1853 (2020).
224. Zhang, X., *et al.* Reversible loss of core–shell structure for Ni–Au bimetallic nanoparticles during CO_2 hydrogenation. *Nat. Catal.* **3**, 411–417 (2020).
225. Ramade, J., *et al.* Tracking the restructuring of oxidized silver-indium nanoparticles under a reducing atmosphere by environmental TEM. **Nanoscale**, **9**, 13563-13574 (2017).
226. Tan, S. F., *et al.* Real-time imaging of nanoscale redox reactions over bimetallic nanoparticles. *Adv. Funct. Mater.* **29**, 1903242 (2019).
227. Xin, H. L., *et al.* Revealing the atomic restructuring of Pt-Co nanoparticles. *Nano Lett.* **14**, 3203-3207 (2014).
228. Chee, S.W., Tan, S.F., Baraissov, Z., Bosman, M., & Mirsaidov, U. Direct observation of the nanoscale Kirkendall effect during galvanic replacement reactions. *Nat. Commun.* **8**, 1224 (2017).
229. Chee, S.W., *et al.* Interface-mediated Kirkendall effect and nanoscale void migration in bimetallic nanoparticles during interdiffusion. *Nat. Commun.* **10**, 2831 (2019).
230. Vincent, J.L., & Crozier, P.A. Atomic level fluxional behavior and activity of CeO_2-supported Pt catalysts for CO oxidation. *Nat. Commun.* **12**, 5789 (2021).
231. Simonsen, S. B., Chorkendorff, I., Dahl, S., Skoglundh, M., & Helveg, S. Coarsening of Pd nanoparticles in an oxidizing atmosphere studied by in situ TEM. *Surf. Sci.*, **648**, 278-283 (2016).
232. https://www.gatan.com/products/tem-imaging-spectroscopy/k3-camera-0
233. Peña, N. O., *et al.* Morphological and structural evolution of Co_3O_4 nanoparticles revealed by in situ electrochemical transmission electron microscopy during electrocatalytic water oxidation. *ACS Nano* **13**, 11372-11381 (2019).

234. Liao, H.-G., & Zheng, H. Liquid cell transmission electron microscopy *Annu. Rev. Phys. Chem.* **67**, 719-747 (2016).
235. Mirsaidov, U., Patterson, J. P., & Zheng, H. Liquid phase transmission electron microscopy for imaging of nanoscale processes in solution. *MRS Bulletin*, **45**, 704-712 (2020).
236. Ou, Z., Liu, C., Yao, L., & Chen, Q. Nanoscale cinematography of soft matter system under liquid-phase TEM. *Acc. Mater. Res.* **1,** 41-52 (2020).
237. Niu, K., *et al.* Bubble nucleation and migration in a lead-iron hydr(oxide) core-shell nanoparticle. *Proc. Natl. Acad. Sci. USA*, **112**, 12928-12932 (2015).
238. Niu, K.-Y., Park, J., Zheng, H., & Alivisatos, A. P. Revealing bismuth oxide hollow nanoparticle formation by the Kirkendall effect. *Nano Lett.* **13**, 5715-5719 (2013).
239. Wu, H. *et al.* Studying reaction mechanisms in solution using a distributed electron microscopy method. *ACS Nano*, **15**, 10296-10308 (2021).
240. A. D. Smigelskas, & E. O. Kirkendall; *Transaction of AIME*, **171** (1947).
241. Wang J.X., *et al.* Kirkendall effect and lattice contraction in nanocatalysts: a new strategy to enhance sustainable activity. *J. Am. Chem. Soc.* **133**, 13551-13557 (2011).
242. Grosse, P., *et al.* Dynamic transformation of cubic copper catalysts during CO_2 electroreduction and its impact on catalytic selectivity. *Nat. Commun.* **12**, *12*, 6736 (2021).
243. LaGrow, A. P., Ward, M. R., Lloyd, D. C., Gai, P. L., & Boyes, E. D. Visualizing the Cu/Cu_2O interface transition in nanoparticles with environmental scanning transmission electron microscopy. *J. Am. Chem. Soc.* **139**, 179-185 (2017).
244. Avanesian, T., *et al.* Quantitative and atomic-scale view of CO-induced Pt nanoparticle surface reconstruction at saturation coverage via DFT calculations coupled with in situ TEM and IR. *J. Am. Chem. Soc.* **139**, 4551-4558 (2017).
245. Chmielewski, A., *et al.* Reshaping dynamics of gold nanopartidcles under H_2 and O_2 at atmospheric pressure. *ACS Nano* **13**, 2024-2033 (2019).
246. Altantzis, T., *et al.* Three-dimensional quantification of the facet evolution of Pt nanoparticles in a variable gas environment. *Nano Lett.* **19**, 477-481 (2019).
247. Sharma, V. P., Sharma, U., Chattopadhyay, M., & Shukla, V. N. Advance applications of nanomaterials: A review. *Mater. Today Proc.*, **5**, 6376-6380 (2018).
248. Zhai, W., Srikanth, N., Kong, L. B., & Zhou, K. Carbon nanomaterials in tribology. *Carbon*, **119**, 150-171 (2017).
249. Greeg, J. R., & De Hosson, J. T. M. Plasticity in small-sized metallic systems: Intrinsic verses extrinsic size effect. *Prog. Mater. Sci.*, **56**, 654-724 (2011).
250. Li, Y., Xu, J., & Li, D. Molecular dynamics simulation of nanoscale liquid flows. *Microfluid. Nanofluid. 9*, 1011–1031 (2010).
251. Kim, J., Ou, Z., Jones, M.R., Song, X., & Chen, Q. Imaging the polymerization of multivalent nanoparticles in solution. *Nat. Commun.* **8**, 761 (2017).
252. Kiener, D., Hosemann, P., Maloy, S., A., & Minor, A. M. *In situ* nanocompression testing of irradiated copper. *Nat. Mater.* **10**, 608–613 (2011).
253. Grosso, R. L., *et al.* In situ transmission electron micrscopy for ultrahigh temperature mechanical testing of ZrO_2. *Nano Lett.* **20**, 1041-1046 (2020).
254. Tian, L., *et al.* Approaching the ideal elastic limit of metallic glasses. *Nat. Commun.* **3**, 609 (2012).
255. Minor, A. M., *et al.* A new view of the onset of plasticity during the nanoindentation of aluminium. *Nat. Mater.* **5**, 697–702 (2006).
256. Jiang, L., *et al.* Visualization and validation of twin nucleation and early-stage growth in magnesium. *Nat. Commun.* **13**, 20 (2022).
257. Kwon, O.-H., Barwick, B., Park, H. S., Baskin, J. S., & Zewail, A. H. Nanoscale mechanical drumming visualized by 4D electron microscopy. *Nano Lett.* **8**, 3557-3562 (2008).
258. Flannigan, D. J., Samartzis, P. C., Yurtsever, A., & Zewail, A. H. Nanomechanical motions of cantilevers: Direct imaging in real space and time with 4D microscopy. *Nano Lett.* **9**, 875-881 (2009).
259. Baskin, J. S., Park, H. S., & Zewail, A. H. Nanomuscial systems visualized and controlled in 4D electron microscopy. *Nano Lett.* **11**, 2183-2191 (2011).
260. Fitzpatrick, A. W. P., Park, S. T., & Zewail, A. H.; Exceptional rigidity and biomechanics of amyloid revealed by 4D electron microscopy. *Proc. Natl. Acad. Sci. USA*, **110**, 10976-10981 (2013).

261. Fitzpatrick, A. W. P., Vanacore, G. M., & Zewail, A. H. Nanomechanics and intermolecular forces of amyloid revealed by four-dimensional electron microscopy. *Proc. Natl. Acad. Sci. USA*, **112**, 3380-3385 (2015).
262. Kim, Y.-J., Lee, Y., Kim, K., Kwon, O.-H. Light-induced anisotropic morphological dynamics of black phosphorus membranes visualized by dark-field ultrafast electron microscopy. *ACS Nano* **14**, 11383-11393 (2020).
263. Lorenz, U. J., & Zewail,A. H.; Biomechanics of DNA structures visualized by 4D electron microscopy. *Proc. Natl. Acad. Sci. USA*, **110**, 2822-2827 (2013).
264. Flannigan, D. J., Park, S. T., & Zewail, A. H. Nanofriction visualized in space and time by 4D electron microscopy. *Nano Lett.* **10**, 4767-4773 (20120).
265. Dai, Z., *et al.* Surface buckling of black phosphorus: Determination, origin, and influence on electronic structure. *Phys. Rev. Mater.* **1**, 074003 (2017).
266. Kavokine, N., Bocquet, M. L. & Bocquet, L. Fluctuation-induced quantum friction in nanoscale water flows. *Nature.* **602**, 84–90 (2022).
267. Liao, H.-G., Niu, K., & Zheng, H., Observation of growth of metal nanoparticles. *Chem. Comm*. **49** 11720-11727 (2013).
268. Tan, S. F., Chee, S. W., Lin, G., & Mirsaidov, U. Direct observation of interactions between nanoparticles and nanoparticle self-assembly in solution. *Acc. Chem. Res.* **50**, 1303-1312 (2017).
269. Luo, B., Smith, J. W., Ou, Z., Chen, Q. Quantifying the self-assembly behavoir of anisotropic nanoparticles using liquid-phase transmission electron microscopy. *Acc. Chem. Res.* **50**, 1125-1133 (2017).
270. Powers, A. S., *et al.* Tracking nanoparticle diffusion and interaction during self-assembly in a liquid cell. *Nano Lett.* **17**, 15-20 (2017).
271. Sutter, E., *et al.*. *In situ* microscopy of the self-assembly of branched nanocrystals in solution. *Nat. Commun.* **7**, 11213 (2016).
272. Chee, S. W., Anand, U., Bisht, G., Tan, S. F., & Mirsaidov, U. Direct observation of the rotation and translation of anisotropic nanoparticles adsorbed at a liquid-solid interface, *Nano Lett.* **19**, 2871-2878 (2019).
273. Paxton, W. F., *et al.* Catalytic nanomotors: Autonomous movement of striped nanorods. *J. Am. Chem. Soc.* **126**, 13424-13431 (2004).
274. Fu, X., Chen, B., Tang, J., & Zewail, A. H. Photoinduced nanobubble-driven superfast diffusion of nanoparticles imaged by 4D electron microscopy, *Sci. Adv.*, **3**, e1701160 (2017).
275. Xu, L., Mou, F., Gong, H., Luo, M., & Guan, J. Light-driven micro/nanomotors: from fundamentals to application. *Chem. Soc. Rev*. **46**, 6905-6926 (2017).
276. Idrobo, J. C. A new resolution quest in electron microscopy. *Nat. Rev. Mater.* **6**, 100-102 (2021).
277. Jiang, Y., *et. al.* Electron ptychography of 2D materials to deep sub-angstom resolution. *Nature*, **559**, 343-349 (2018).
278. Chen, Z. *et. al* Electron ptychography achieves atomic-resolution limits set by lattice vibrations. *Science*, **372**, 826-831 (2021).
279. Krivanek, O. L., *et. al.* Progress in ultrahigh energy resolution EELS. *Ultramicroscopy*, **203**, 60-67 (2019).
280. Crozier, P. A. *et al.* Workshop Report on Enabling Transformative Advances in Energy and Quantum Materials through Development of Novel Approaches to Electron Microscopy. **2021.**
281. Priebe, K. E., *et. al.* Attosecond electron pulse trains and quantum state reconstruction in ultrafast transmission electron microscopy. *Nature Photonics*, **11**, 7930797 (2017).
282. Morimoto, Y., & Baum, P. Diffraction and microscopy with attosecond electron pulse trains. *Nature Physics*, **14**, 252-256 (2018).
283. Baum, P. & Krausz, F. Capturing atomic-scale carrier dynamics with electrons. *Chem. Phys. Lett.* **683**, 57-61 (2017).
284. Baum, P. & Zewail, A. H. Attosecond electron pulses for 4D diffraction and microscopy. *Proc. Natl. Acad. Sci. USA,* **104**, 18409-18414 (2007).

Highlighted references

8. Heo, J., Dummett Torres, D., Banerjee, P., & Jain, P. K. In-situ electron microscopy mapping of an order-disorder transition in a superionic conductor. *Nat Commun.* **10,** 1505 (2019). **Real time, second timescale imaging of the nucleation and propagation of a phase change in nanomaterials, revealing dynamic relationships with crystal structure.**

16. van der Veen, R. M., Kwon, O.-H., Tissot, A., Hauser, A., & Zewail, A. H. Single-nanoparticle phase transitions visualized by four-dimensional electron microscopy. *Nat. Chem.* **5,** 395–402 (2013). **Imaging optically initiated phase transitions in individual metal-organic nanoparticles with sub µs lifetimes.**

24. Kashin, A.S., & Ananikov, V.P. Monitoring chemical reactions in liquid media using electron microscopy. *Nat. Rev. Chem.* **3,** 624–637 (2019). **A thorough review of applications of electron microscopy for monitoring liquid phase reactions.**

53. Vendelbo, S. B., *et al*. Visualization of oscillatory behaviour of Pt nanoparticles catalysing CO oxidation. *Nature Mater.* **13**, 884–890 (2014). **Revealing underlying surface chemistries in catalytic reactions by imaging structural changes on Pt particles during CO oxidation.**

138. Danz, T., Domrose, T., & Ropers, C. Ultrafast nanoimaging of the order parameter in a structural phase transition. *Science*, **371**, 371-374 (2021). **Nanoscale mapping of excited state domains with ps scale lifetimes following optical excitation.**

141. Lorenz, U. J., & Zewail, A. H. Observing liquid flow in nanotubes by 4D electron microscopy. *Science*. **344**, 1496-1500 (2014). **Imaging of fluid behavior at the nanoscale via laser melting of lead within ZnO nanotubes.**

143. Liu, H., *et al.* Visualization of plasmonic couplings using ultrafast electron microscopy. *Nano Lett*. **21,** 5842-5849 (2021). **Imaging ultrafast coupling of electromagnetic fields between nanostructures.**

166. Yang, J., *et al.* Formation of two-dimensional transition metal oxide nanosheets with nanoparticles as intermediates. *Nat. Mater.* **18,** 970–976 (2019). **Imaging the growth of nanostructures starting from nucleation, taking advantage of the high temporal resolution of a direct electron camera.**

Acknowledgements

F.M.A. was supported by the Robert C. and Carolyn J. Springborn Endowment for Student Support Program at UIUC. P.K.J. was supported by a Guggenheim Fellowship. R.M.V. was, in part, supported by a Packard Fellowship in Science and Engineering from the David and Lucile Packard Foundation. We thank the reviewers for their constructive comments.

Author contributions

All authors contributed equally to the preparation of the manuscript.

Competing interests

The authors declare no competing interests.

Graphical abstract

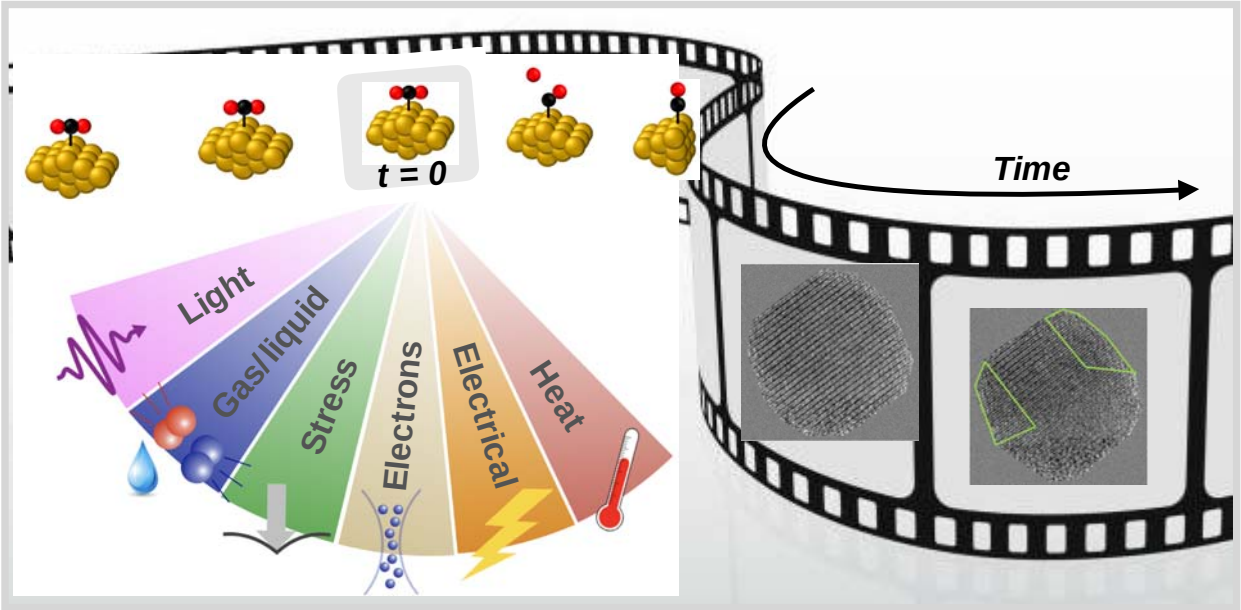

Note: the nanoparticle images on the right-hand side should be wrapped around the movie strip.

Figure legends

Fig. 1. Common types of chemical dynamics, their timescales, and the stimuli and techniques used to probe these dynamics *in situ* with electron microscopy.

Fig. 2. *Methodologies for time-resolved TEM.* **a** Studies involving the application of a constant perturbation/stimulus and continuous electron probing *in situ*. Detector frame rates determine temporal resolution. **b** Studies conducted using pulsed excitation and various probe schemes. (1) Slow dynamics can be recorded with continuous electron probing using fast cameras following the application of a short trigger. (2) For fast irreversible dynamics, images, diffraction patterns, or loss spectra can be captured with a single probe pulse (single-shot mode). Time series are produced by varying the time delay between the pump and probe pulse. Reversible fast and ultrafast dynamics can be recorded with stroboscopy, in which repeated pulsed pump and probe signal are recorded to produce an image. Time series are produced by varying the time delay between pump and probe pulses. (3) As an extension of single-shot mode, movie-mode TEM involves multiple probe pulses with differing time delays that are deflected onto different regions of the camera. (4) Pump–probe stroboscopy at high repetition rates is used to record ultrafast dynamics on the fs–ps timescale. The pump-induced dynamics needs to be reversible in this case.

Fig. 3. *Phase transformation dynamics probed by time-resolved TEM imaging, diffraction, and spectroscopy.* **A** Electron-beam induced transition from a low-temperature, vacancy-ordered (VO) phase to a high-temperature, disordered superionic (SI) phase in a single Cu_2Se nanoparticle over the course of seconds. Crystallographic nucleation and phase propagation are studied in real time. Scale bar is 5 nm. Adapted from ref. 8 **b** Single-shot electron diffraction and energy-loss spectroscopy of irreversible photothermal reduction of NiO to metallic Ni nanoparticles on the nanosecond–microsecond time scale. Scale bar is 10 nm^{-1}. Adapted from ref. 102. **C** Ultrafast pump-probe dark field imaging of a light-induced charge-density wave phase transition from a non-commensurate (NC) phase to an incommensurate (IC) phase in TaS_2 on the fs–ps time scale. Adapted from ref. 138.

Fig. 4. *Charge/heat transfer dynamics and imaging of plasmonic fields studied by time-resolved TEM.* **a** (i)–(iii) Time-series imaging of the sodiation of a CuS electrode in a Na–air battery. Tracking of the reaction front provides insight into the transfer of Na^+ and activation of the electrode material. Adapted from ref. 190 (iv)–(vi) Snapshots of the sodiation of a SnSb electrode for a Na–air battery at –2V vs. Na/Na+. The sodiation kinetics as a function of the applied bias reveals Na^+ diffusion coefficients. Adapted from ref. 197. **b** Ultrafast imaging of coupling between evanescent fields of a Au nanorod and a graphene step edge (iv–vi) and corresponding static images (i–iii). These fields decay within 1 ps. The double arrow labeled with *E* denotes the light polarization direction. The electron energy-loss spectrum on the right indicates that electrons, which have gained energy during the interaction with the laser, are used for imaging. Scale bar is 200 nm. Adapted from ref. 143. **c** Phonon dynamics in bilayer MoS_2. (i) Static bright-field image with regions of interest (ROI) 1 and 2 indicated. (ii) The integrated intensity in ROIs 1 and 2 as a function of time delay. TEM reveals how nanostructural defects (step edges) affect phonon modes and cause dephasing of vibrations between the layers (bottom image). Scale bar is 500 nm. Adapted from ref. 201.

Fig. 5. *Restructuring dynamics of individual nanoparticles.* **a** *In situ* ETEM image time-series of CeO_2-supported Pt nanoparticles at elevated temperature and under CO and O_2 exposure. (i) Time-averaged image of the catalyst obtained by summing together the individual 0.5 s exposure frames over the entire [0–2.0] s acquisition period. (ii)–(v) Atomic-scale structural dynamics that evolve over 0.5 s intervals from t = 0 s to t = 2.0 s. (vi) High-resolution TEM image of a typical Pt nanoparticle supported on a (111) surface of a CeO_2 nanoparticle, with indices of exposed Pt surfaces marked in the image. Adapted from ref. 230.**b** Time series showing reshaping of Pt nanoparticles. Reversible faceting is observed at intermediate time scales, which is related to the oscillatory catalytic CO oxidation. Adapted from ref 53 **c** Amorphization of the surface of TiO_2 nanoparticles in operando during photocatalytic water splitting. Adapted from ref. 40. **d** Time-resolved imaging of void formation in and hollowing of Ag nanoparticles during the galvanic exchange reaction with Au^{3+} in solution. Adapted from ref. 228.

Fig. 6. *Time-resolved TEM imaging of nanomechanical dynamics.* **a** Dark-field micrographs at select time-points and cross-section profiles of the diffraction intensity, formed by selecting the (200) diffraction spot, for black phosphorous following ns-pulsed excitation. Bottom: morphology reconstructed from the dark-field micrographs. Adapted from ref 262 **b** (i) Single-shot imaging of fast photothermal melting of lead within ZnO nanotubes (55 nm diameter). When heated with a single laser pulse, the lead column expands on the ns time scale (ii) before returning to its original

length at longer times (iii). The coefficient of friction and slip length were determined by fitting the expansion and contraction dynamics. (iv) and (v) Numerical simulations for two different column lengths, *l*, where the parameters of the simulation have been adjusted to match the experiment. Scale bar is 200 nm. Adapted from ref. 141.

Fig. 7 *Key goals, enabling technologies, and "dream" experiments that drive the future development of time-resolved in situ TEM.*

Short (40 word) summary

Adding temporal resolution to atomic-scale imaging represents the last dimensional frontier in transmission electron microscopy (TEM). This Review highlights recent key technical advances and applications of time-resolved TEM to the study of nanoscale dynamics of chemical processes on a broad range of timescales ranging from femtoseconds to minutes.

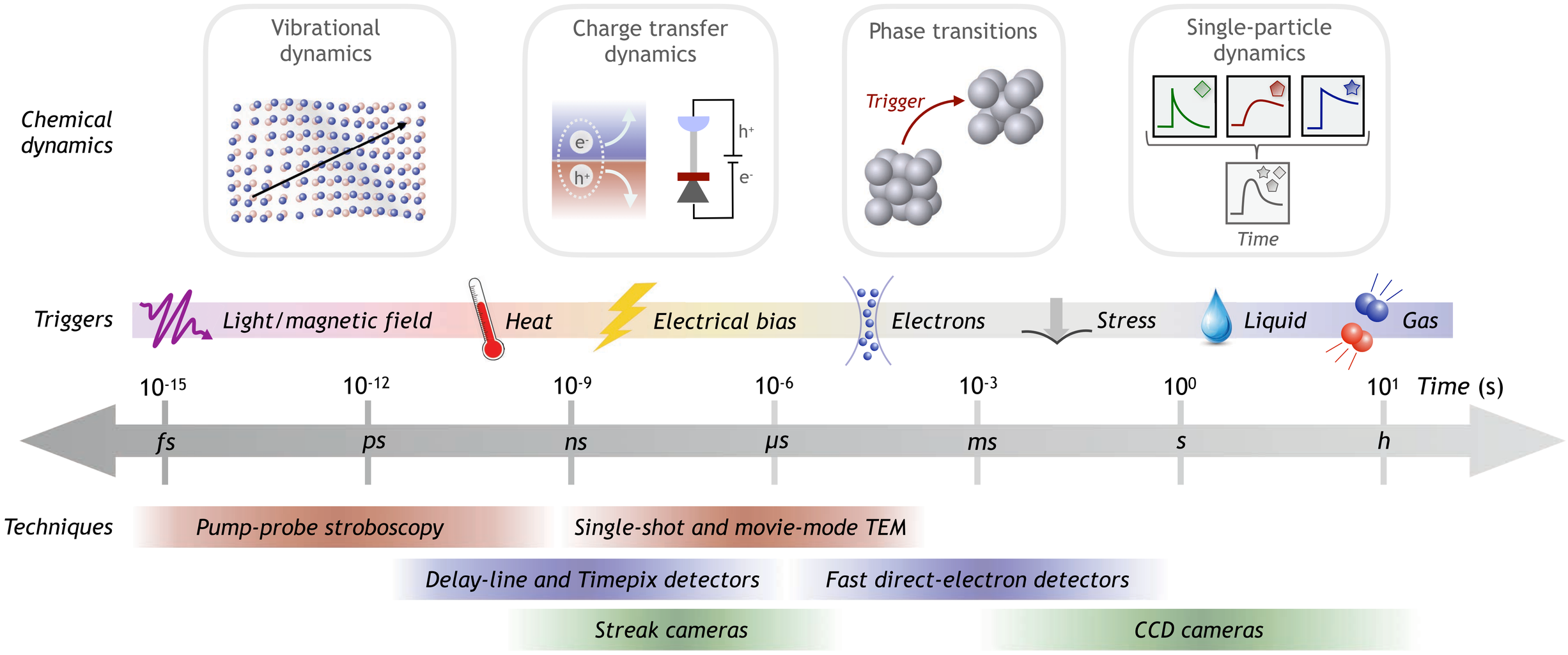
Chemical dynamics
Vibrational dynamics
Charge transfer dynamics
e-
h+
h+
e-
Phase transitions
Trigger
Single-particle dynamics
Time
Triggers
Light/magnetic field
Heat
Electrical bias
Electrons
Stress
Liquid
Gas
10-15
10-12
10-9
10-6
10-3
100
101
Time (s)
fs
ps
ns
μs
ms
s
h
Techniques
Pump-probe stroboscopy
Single-shot and movie-mode TEM
Delay-line and Timepix detectors
Fast direct-electron detectors
Streak cameras
CCD cameras

Figure 1

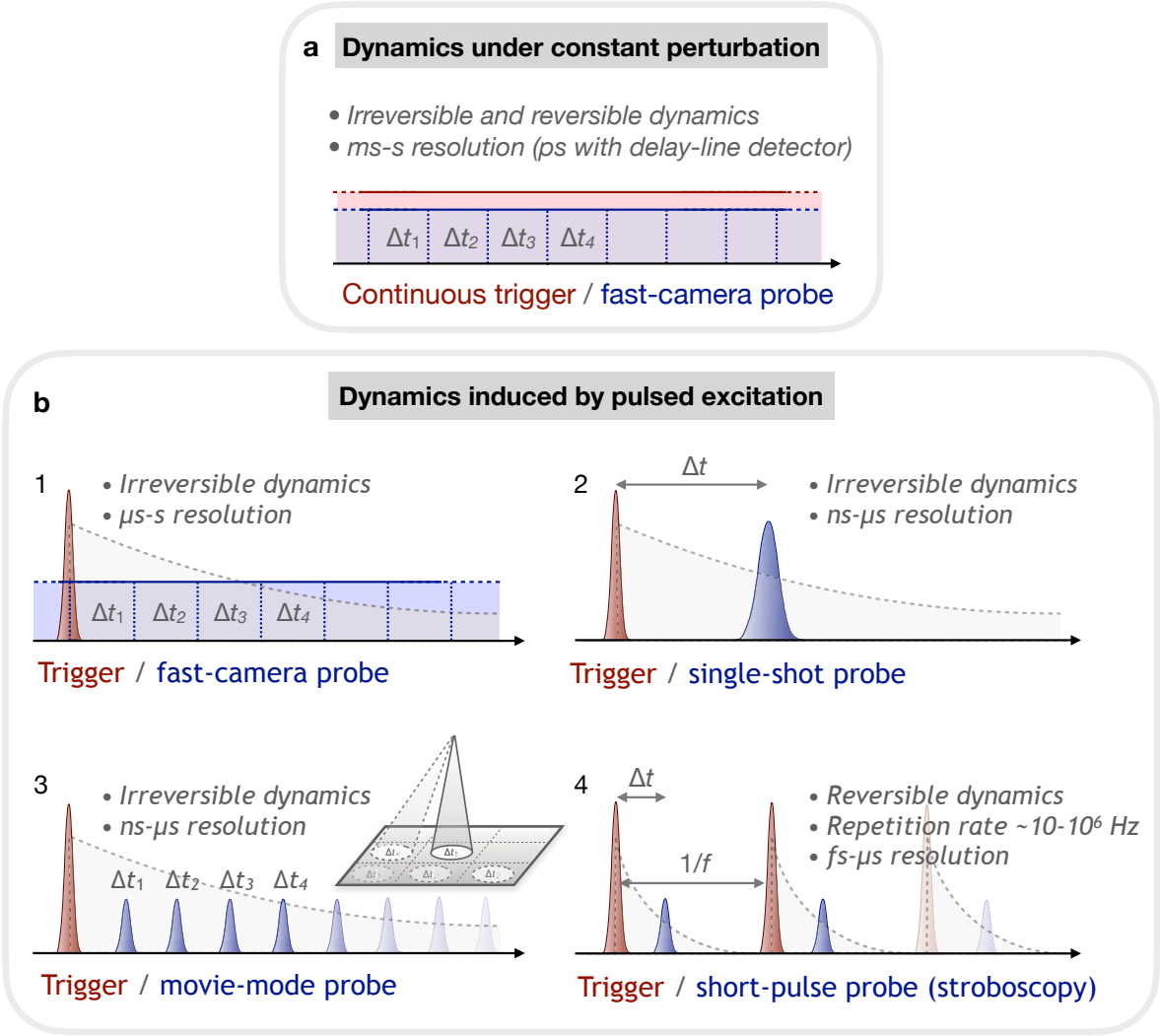
a
Dynamics under constant perturbation
• Irreversible and reversible dynamics
• ms-s resolution (ps with delay-line detector)
Δt1 Δt2 Δt3 Δt4
Continuous trigger / fast-camera probe
b
Dynamics induced by pulsed excitation
1
• Irreversible dynamics
• μs-s resolution
Δt1 Δt2 Δt3 Δt4
Trigger / fast-camera probe
2
Δt
• Irreversible dynamics
• ns-μs resolution
Trigger / single-shot probe
3
• Irreversible dynamics
• ns-μs resolution
Δt1 Δt2 Δt3 Δt4
Trigger / movie-mode probe
4
Δt
1/f
• Reversible dynamics
• Repetition rate ~10-10⁶ Hz
• fs-μs resolution
Trigger / short-pulse probe (stroboscopy)

Figure 2

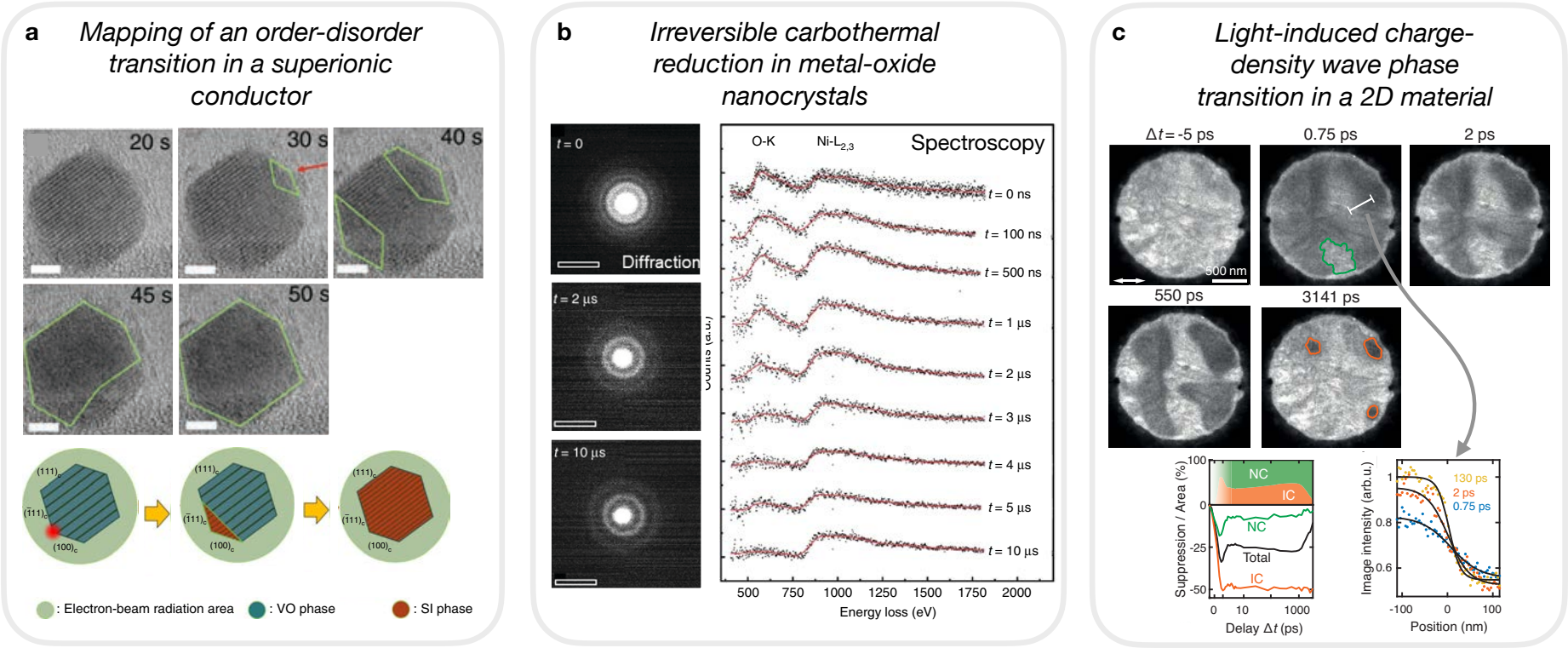
a
Mapping of an order-disorder transition in a superionic conductor
20 s
30 s
40 s
45 s
50 s
: Electron-beam radiation area
: VO phase
: SI phase
b
Irreversible carbothermal reduction in metal-oxide nanocrystals
t = 0
Diffraction
t = 2 µs
t = 10 µs
O-K
Ni-L2,3
Spectroscopy
t = 0 ns
t = 100 ns
t = 500 ns
t = 1 µs
t = 2 µs
t = 3 µs
t = 4 µs
t = 5 µs
t = 10 µs
500
750
1000
1250
1500
1750
2000
Energy loss (eV)
c
Light-induced charge-density wave phase transition in a 2D material
Δt = -5 ps
0.75 ps
2 ps
500 nm
550 ps
3141 ps
NC
IC
Total
Suppression / Area (%)
Delay Δt (ps)
130 ps
2 ps
0.75 ps
Image intensity (arb.u.)
Position (nm)

Figure 3

a *Mapping of an order-disorder transition in a superionic conductor*

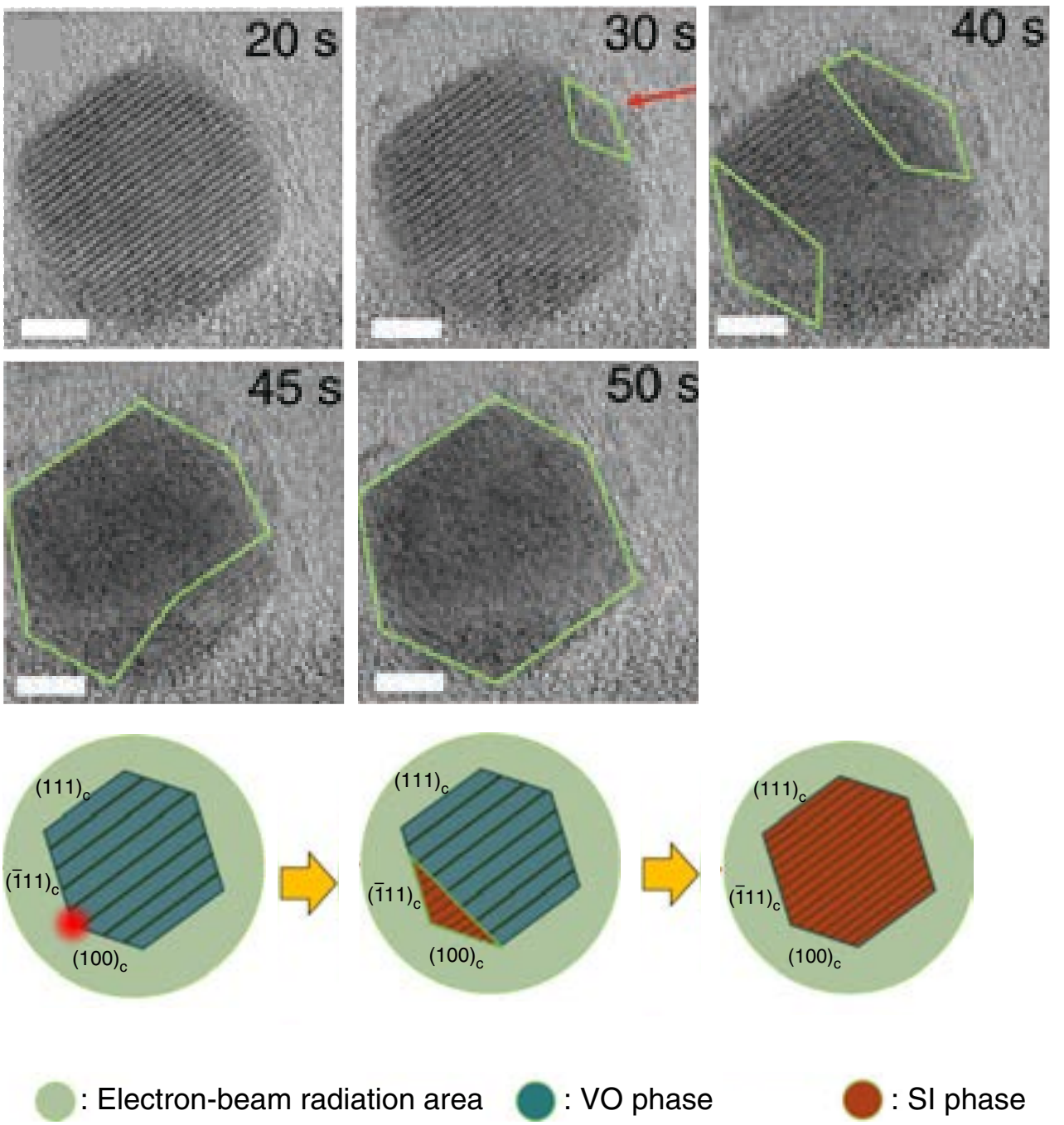

Fig. 3a

b *Irreversible carbothermal reduction in metal-oxide nanocrystals*

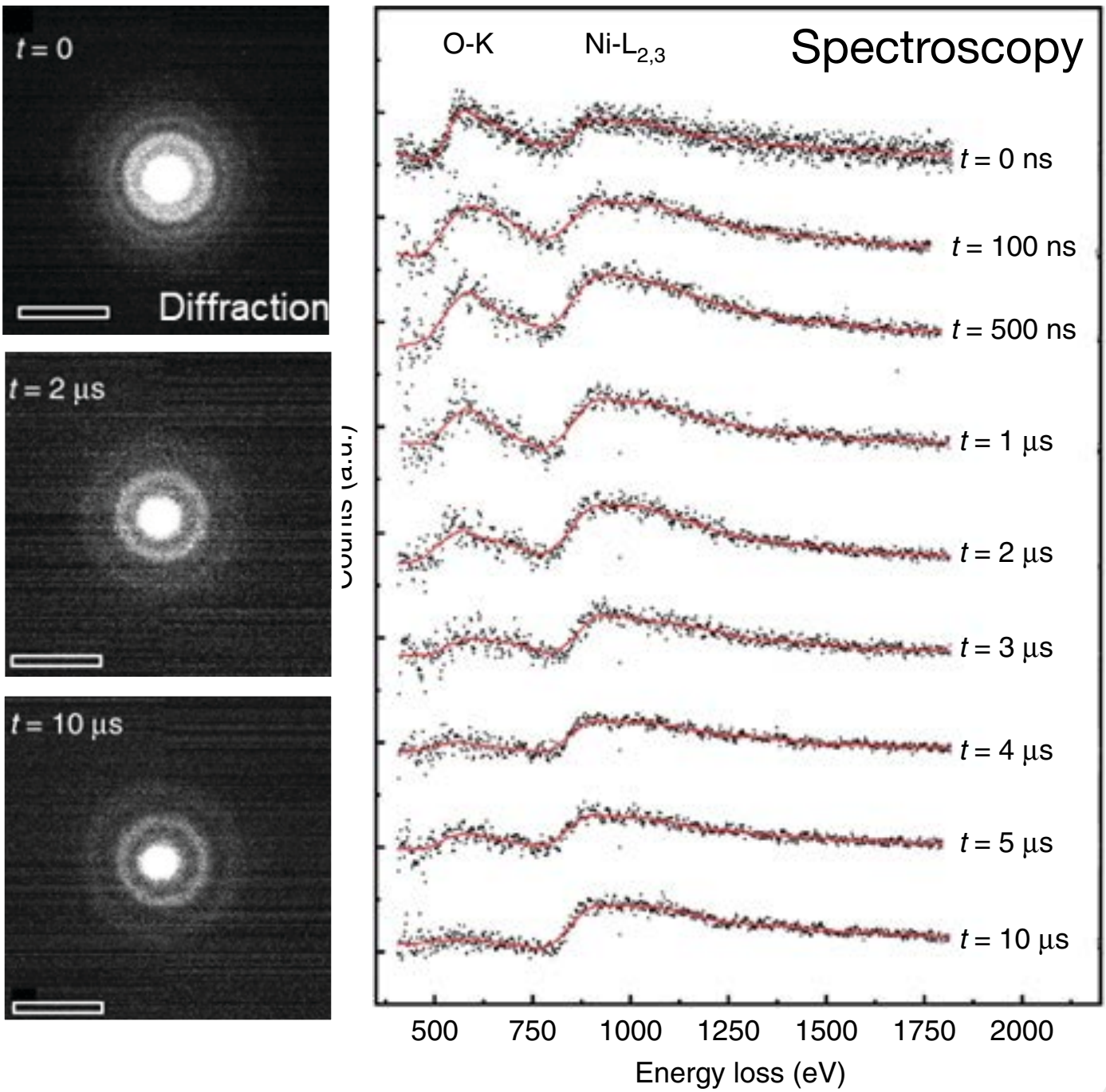

Fig. 3b

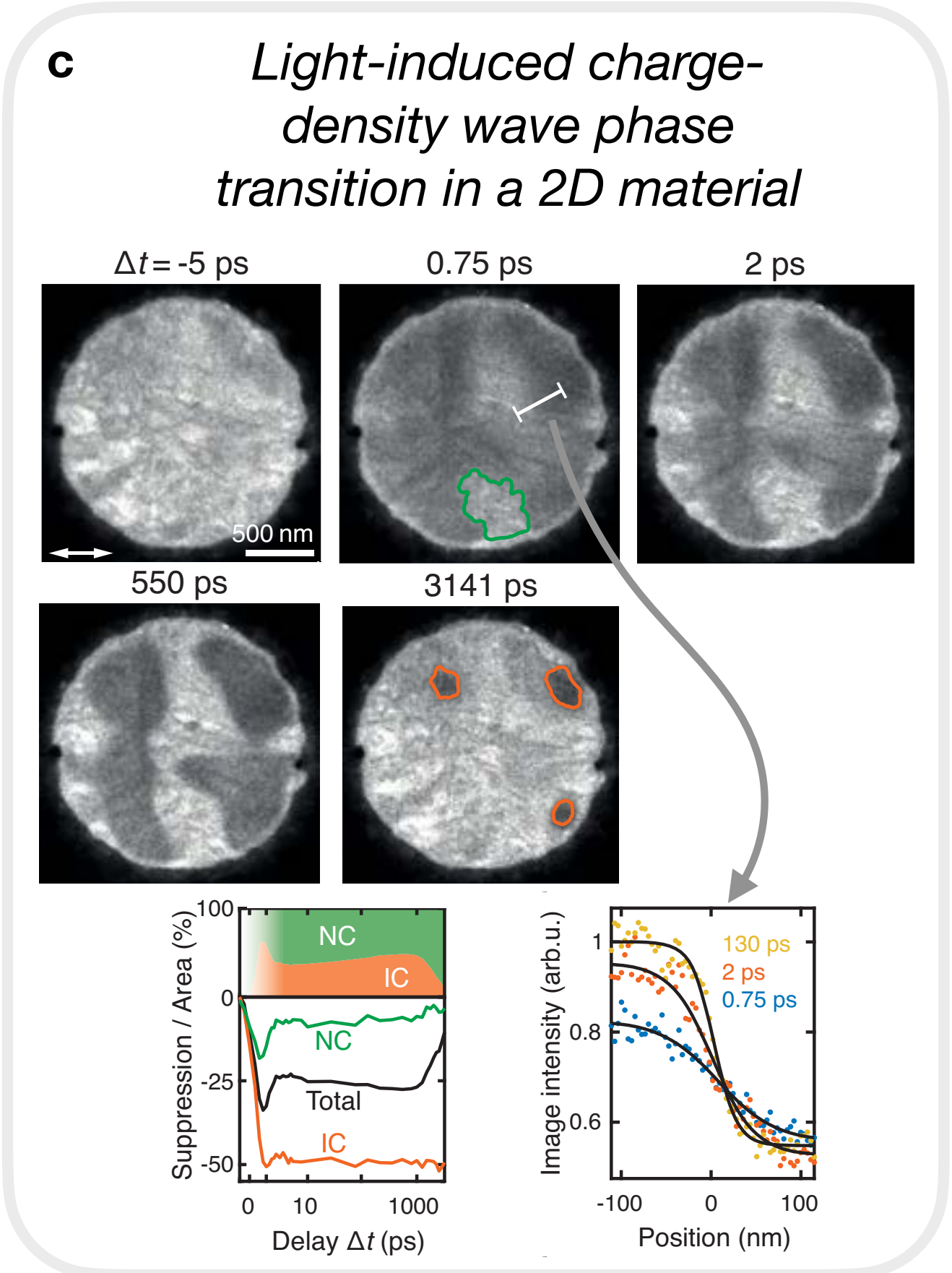
c
Light-induced charge-density wave phase transition in a 2D material
Δt = -5 ps
0.75 ps
2 ps
500 nm
550 ps
3141 ps
NC
IC
NC
Total
IC
Suppression / Area (%)
100
0
-25
-50
0
10
1000
Delay Δt (ps)
130 ps
2 ps
0.75 ps
Image intensity (arb.u.)
1
0.8
0.6
-100
0
100
Position (nm)

Fig. 3c

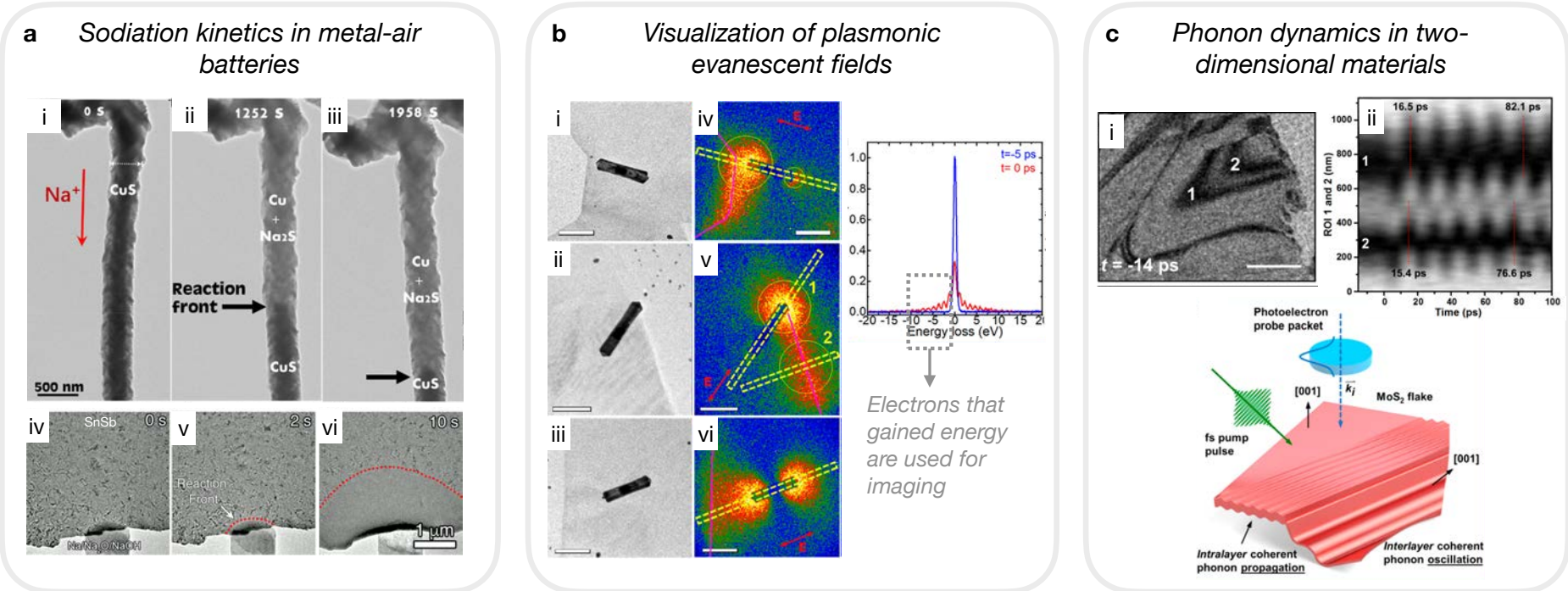
a
Sodiation kinetics in metal-air batteries
i
0 s
ii
1252 s
iii
1958 s
Na+
CuS
Cu
+
Na2S
Reaction front
500 nm
iv
SnSb
0 s
v
2 s
Reaction Front
vi
10 s
1 μm
b
Visualization of plasmonic evanescent fields
t=-5 ps
t= 0 ps
Energy loss (eV)
Electrons that gained energy are used for imaging
c
Phonon dynamics in two-dimensional materials
t = -14 ps
16.5 ps
82.1 ps
15.4 ps
76.6 ps
ROI 1 and 2 (nm)
Time (ps)
Photoelectron probe packet
MoS2 flake
fs pump pulse
[001]
Intralayer coherent phonon propagation
Interlayer coherent phonon oscillation

Figure 4

a *Sodiation kinetics in metal-air batteries*

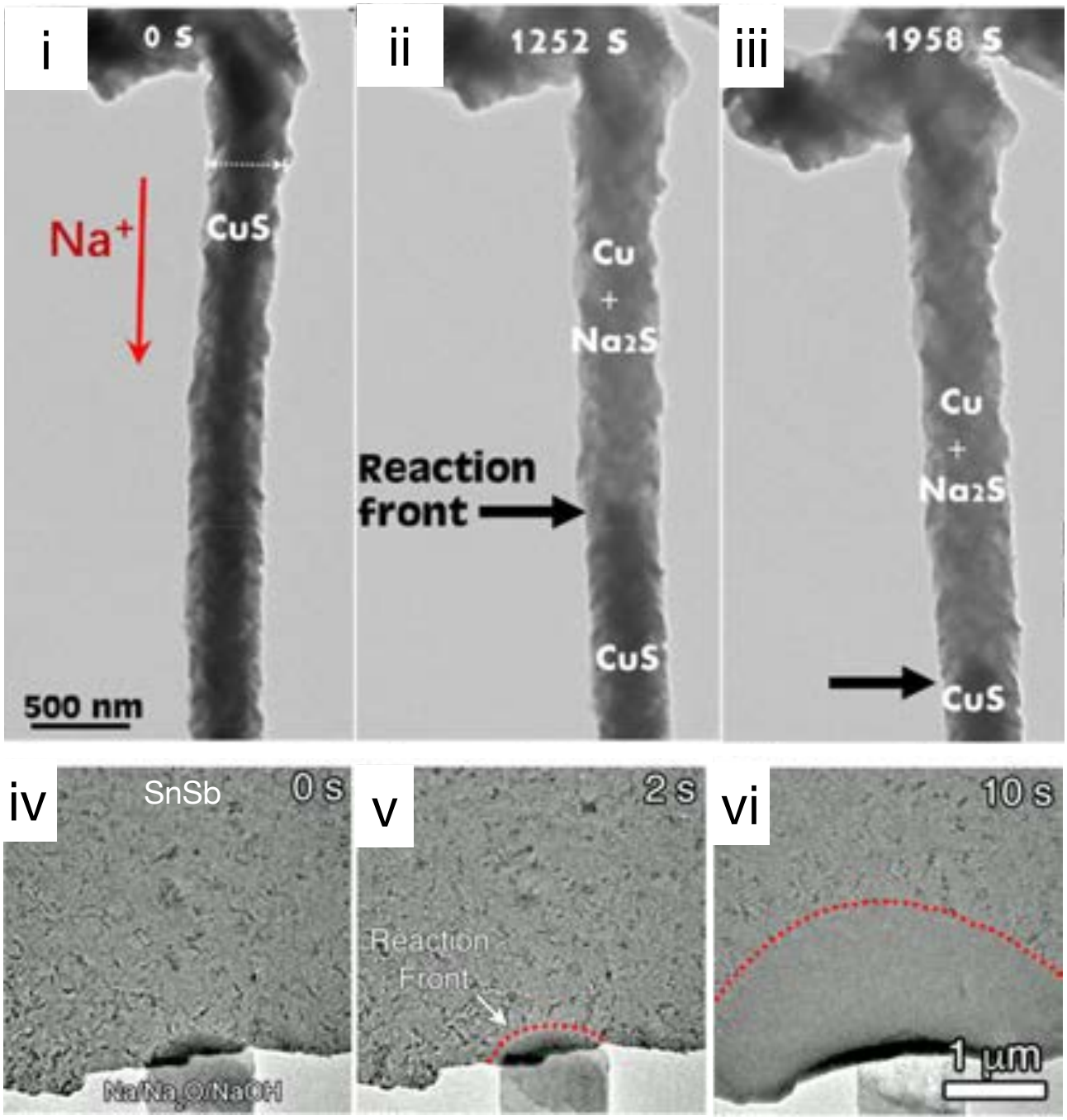

Fig. 4a

b *Visualization of plasmonic evanescent fields*

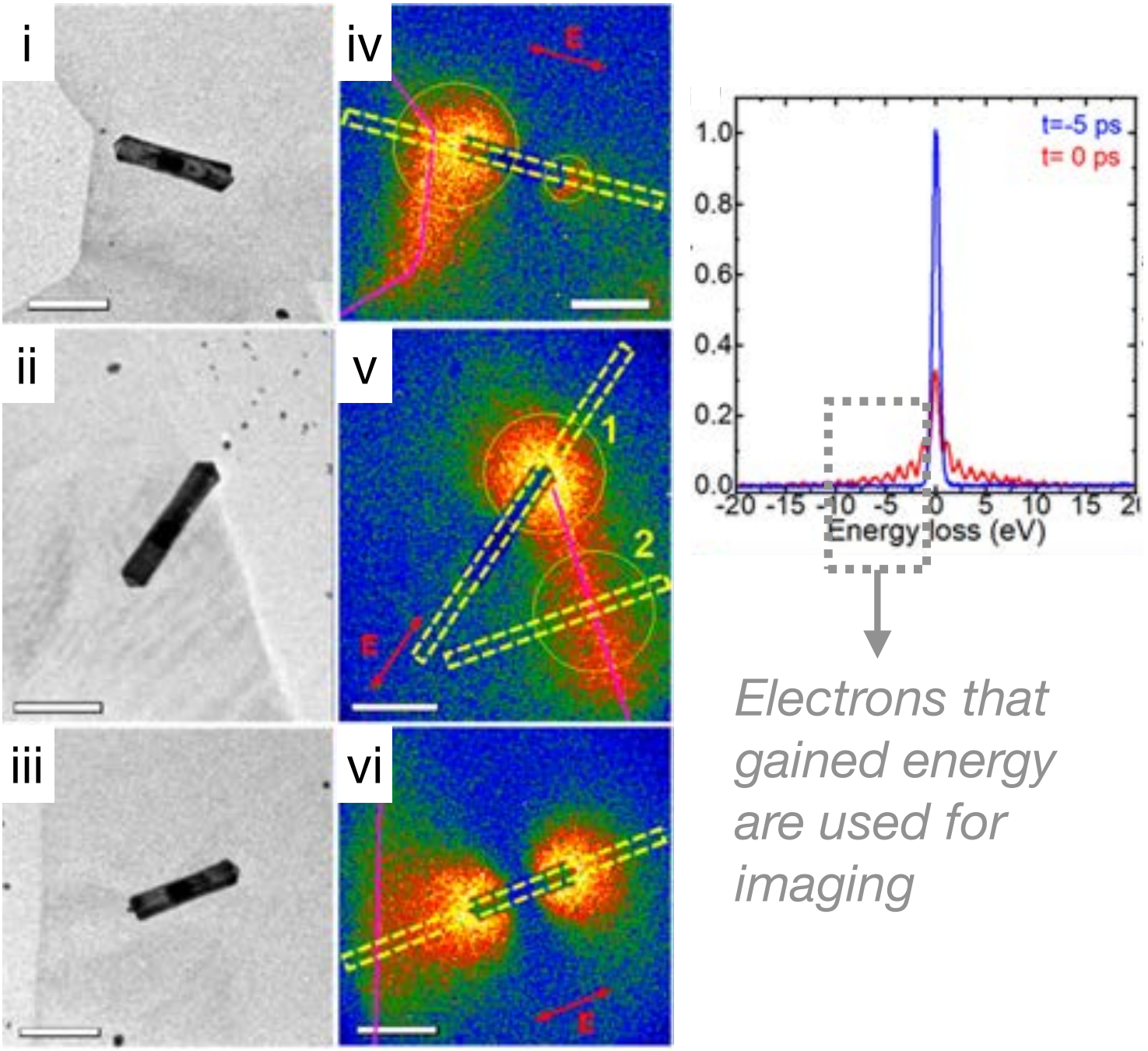

Electrons that gained energy are used for imaging

Fig. 4b

c *Phonon dynamics in two-dimensional materials*

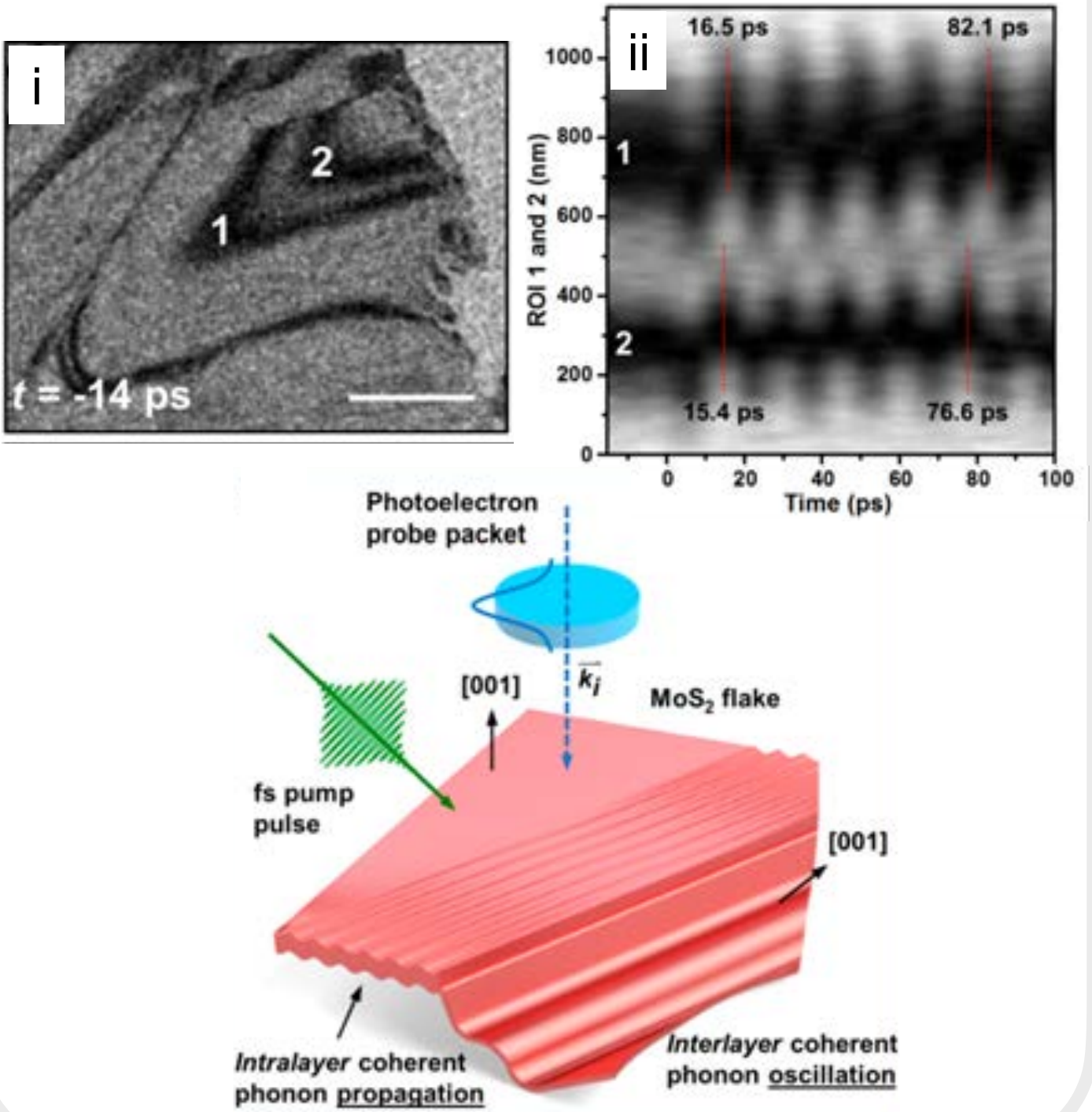

Fig. 4c

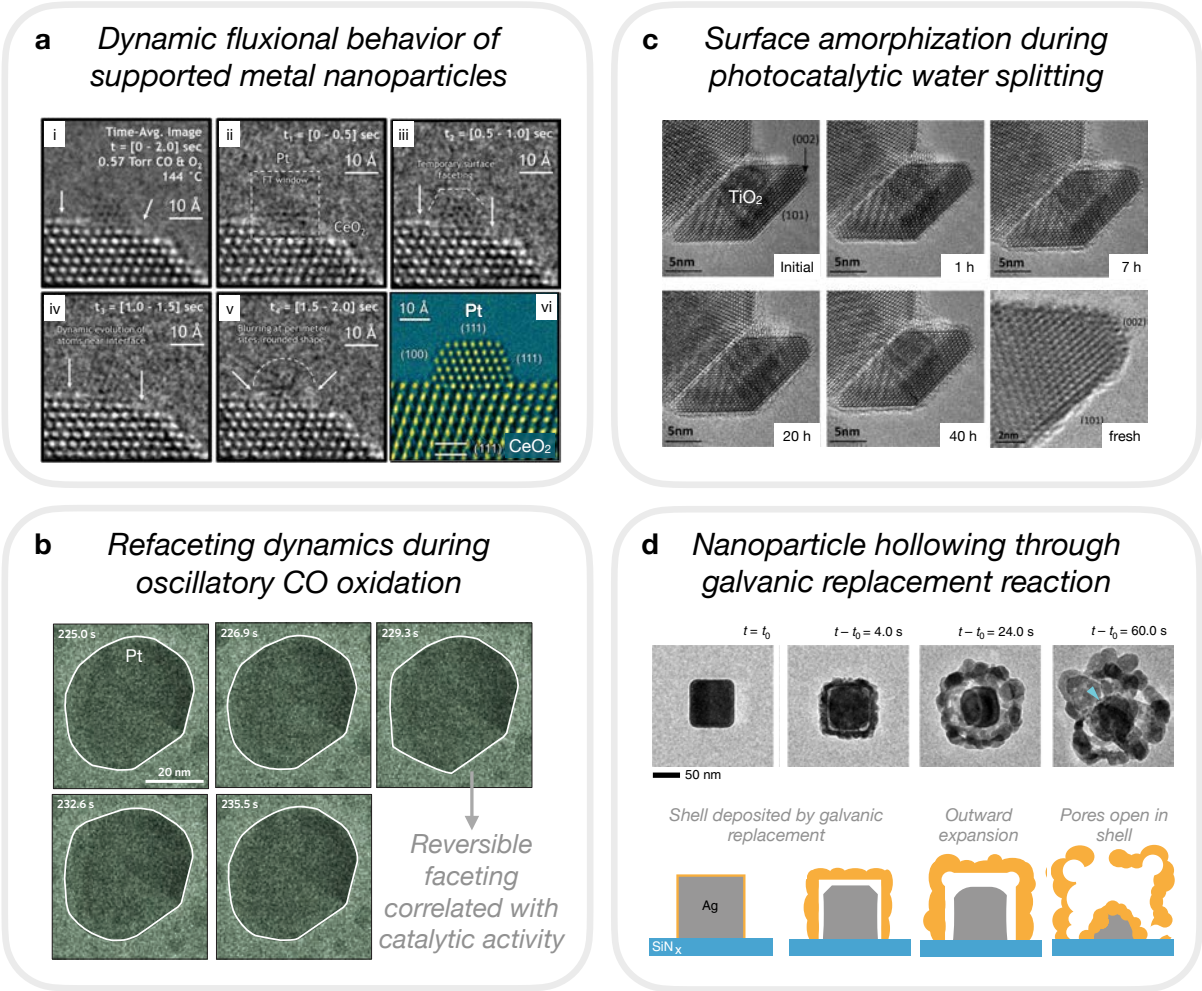
a
Dynamic fluxional behavior of supported metal nanoparticles
Time-Avg. Image
t = [0 - 2.0] sec
0.57 Torr CO & O2
144 °C
10 Å
Pt
CeO2
Temporary surface faceting
Dynamic evolution of atoms near interface
Blurring at perimeter sites, rounded shape
(111)
(100)
(111) CeO2
c
Surface amorphization during photocatalytic water splitting
TiO2
(002)
(101)
5nm
Initial
1 h
7 h
20 h
40 h
fresh
2nm
b
Refaceting dynamics during oscillatory CO oxidation
225.0 s
226.9 s
229.3 s
232.6 s
235.5 s
Pt
20 nm
Reversible faceting correlated with catalytic activity
d
Nanoparticle hollowing through galvanic replacement reaction
t = t0
t − t0 = 4.0 s
t − t0 = 24.0 s
t − t0 = 60.0 s
50 nm
Shell deposited by galvanic replacement
Outward expansion
Pores open in shell
Ag
SiNx

Figure 5

a *Dynamic fluxional behavior of supported metal nanoparticles*

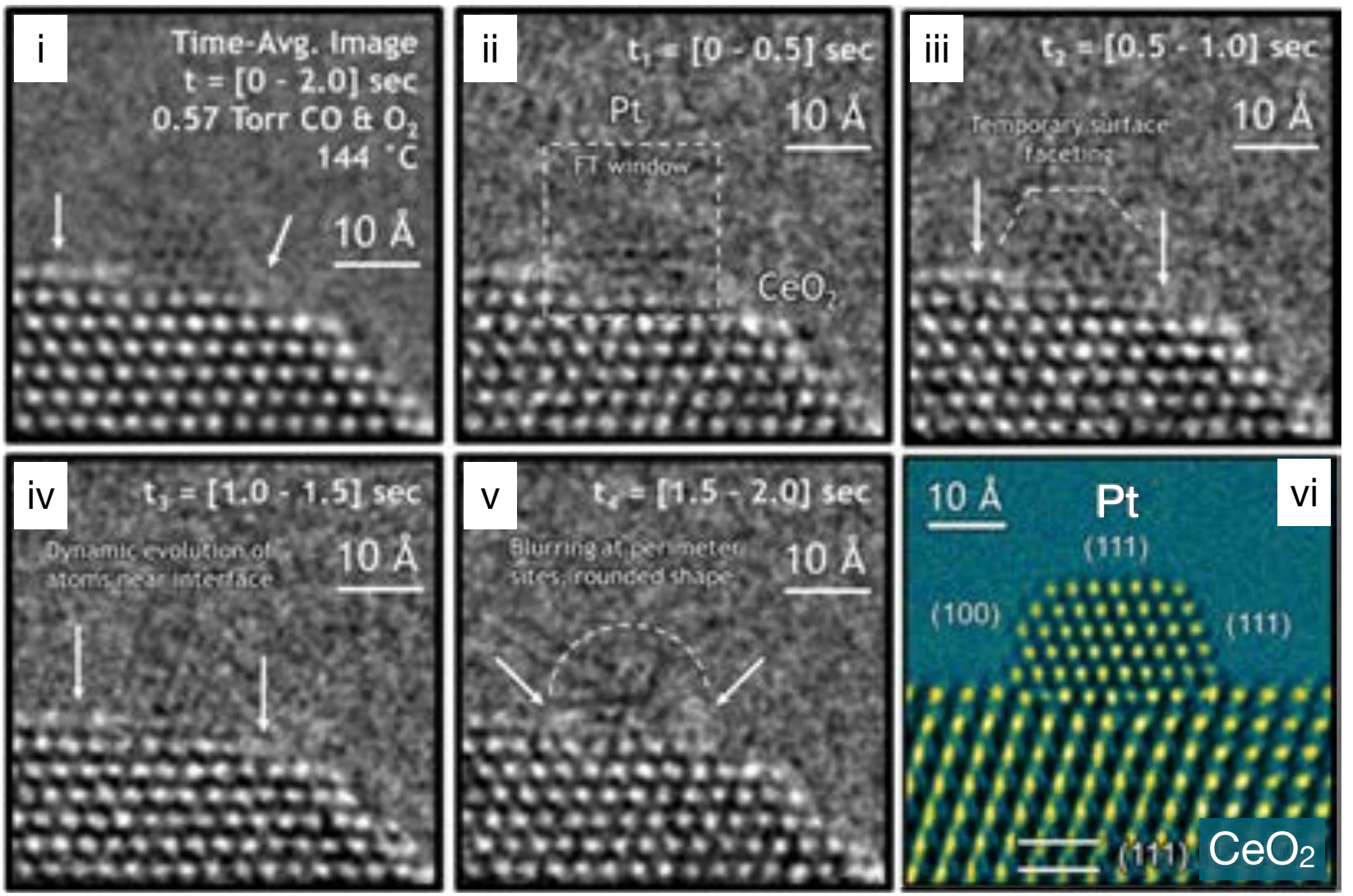

Fig. 5a

b *Refaceting dynamics during oscillatory CO oxidation*

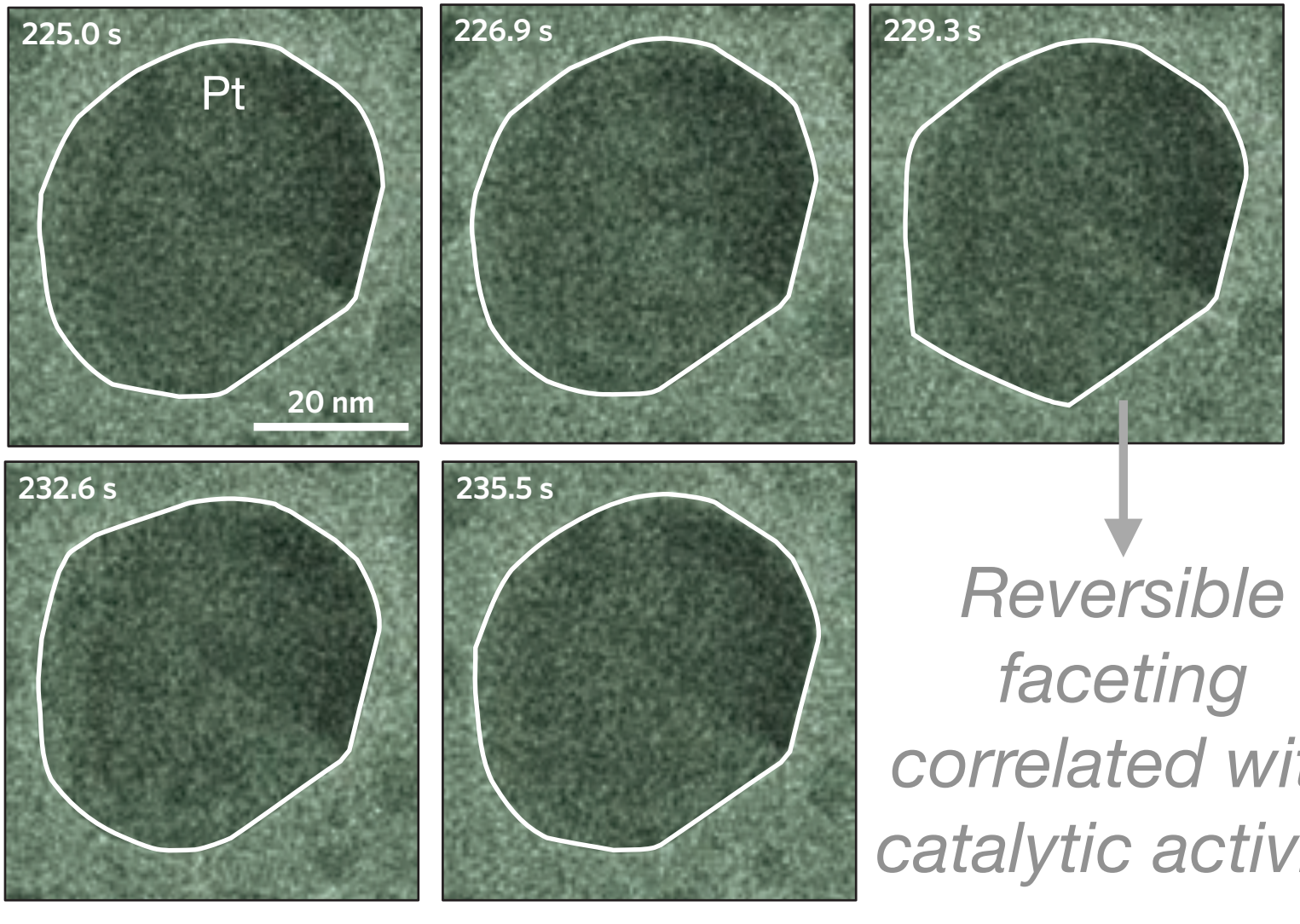

Reversible faceting correlated with catalytic activity

Fig. 5b

c *Surface amorphization during photocatalytic water splitting*

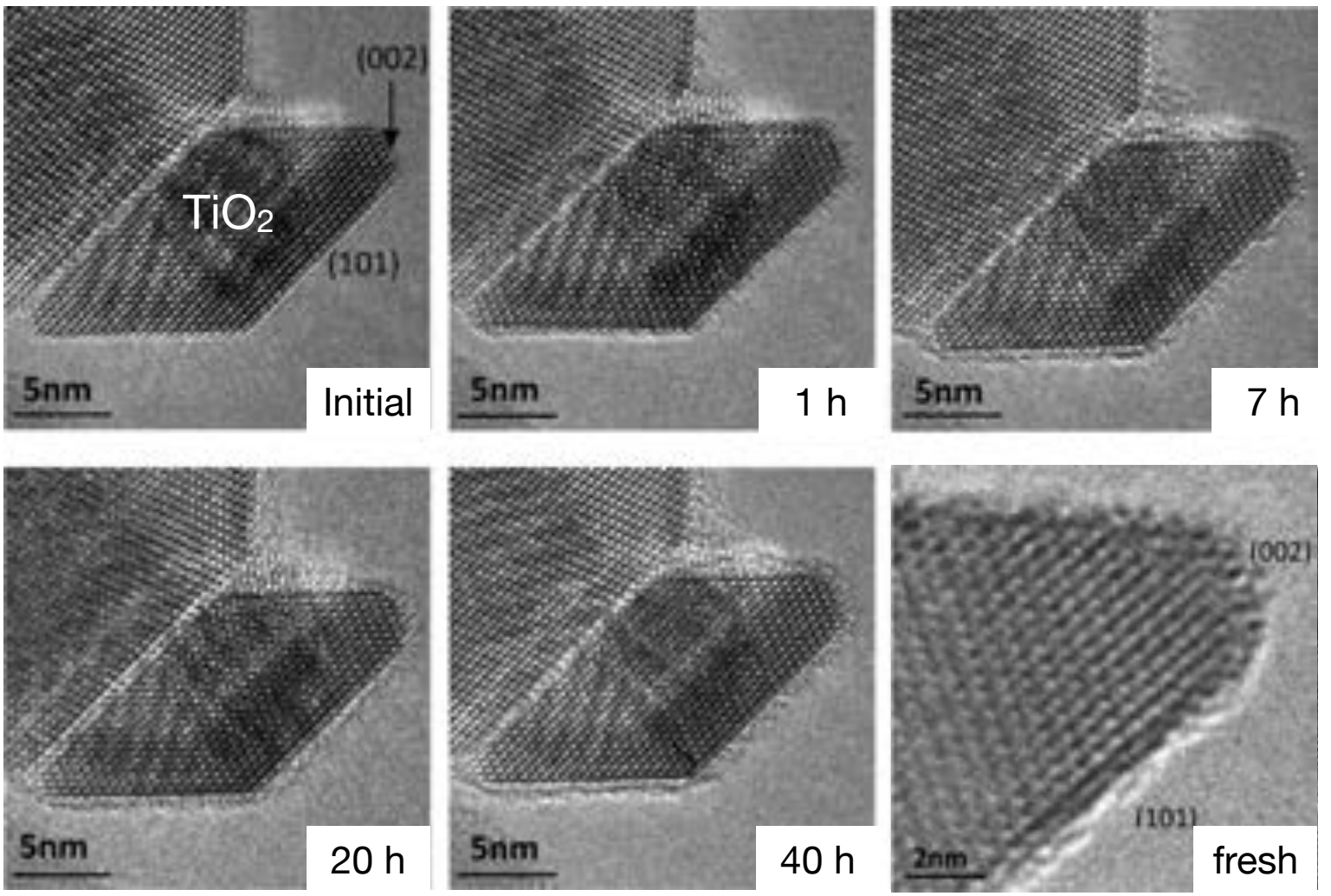

Fig. 5c

d *Nanoparticle hollowing through galvanic replacement reaction*

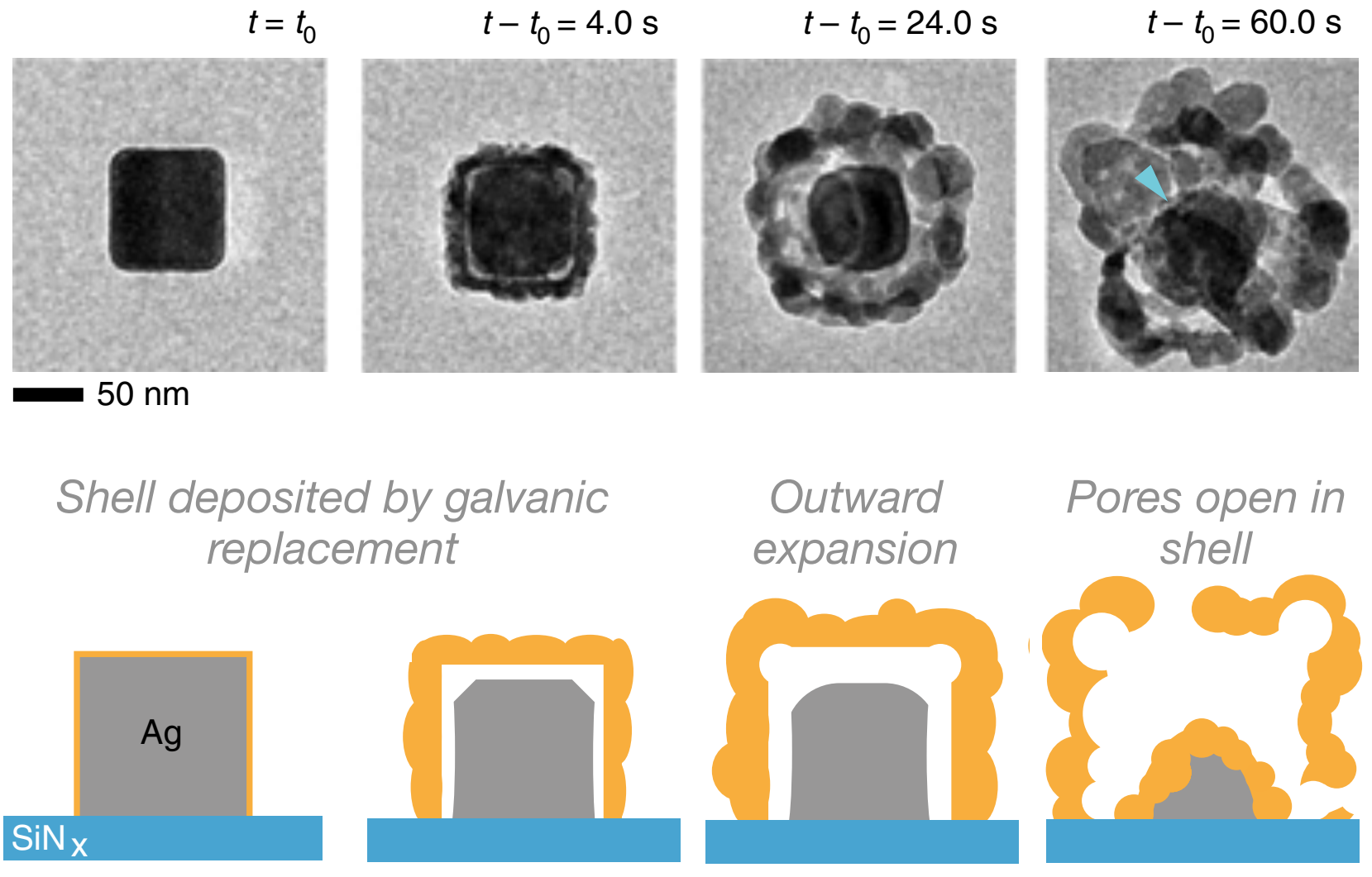

Fig. 5d

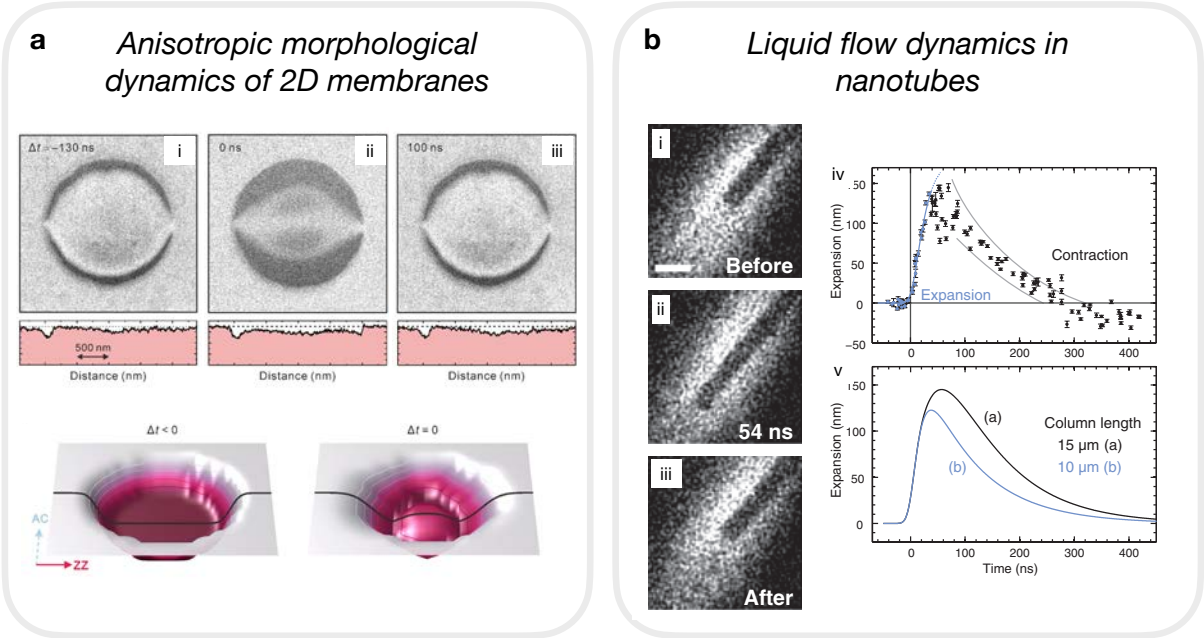
a
Anisotropic morphological dynamics of 2D membranes
i
ii
iii
0 ns
100 ns
500 nm
Distance (nm)
Δt < 0
Δt = 0
AC
ZZ
b
Liquid flow dynamics in nanotubes
Before
54 ns
After
iv
Expansion (nm)
Contraction
Expansion
v
(a)
(b)
Column length
15 μm (a)
10 μm (b)
Time (ns)

Figure 6

a *Anisotropic morphological dynamics of 2D membranes*

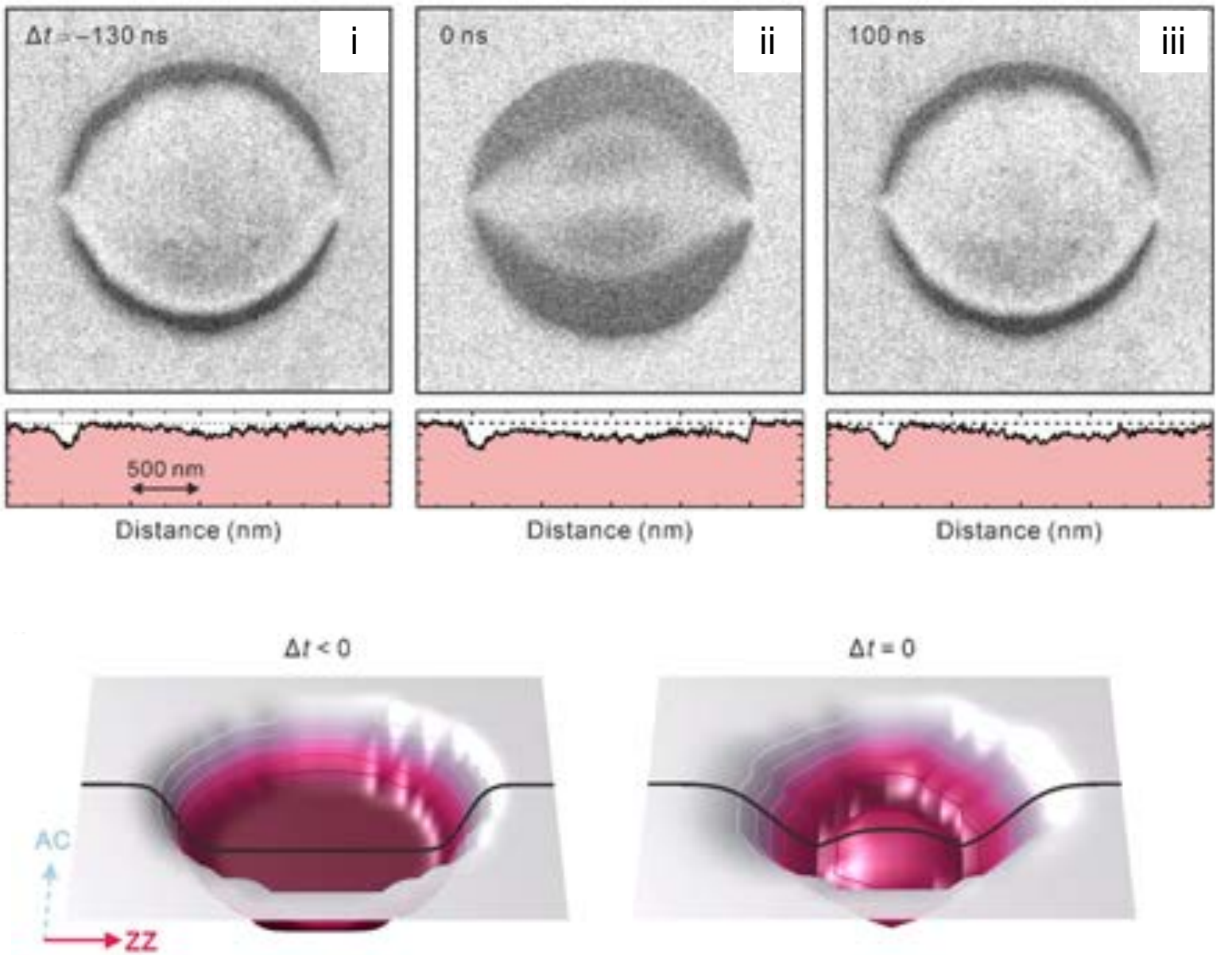

Fig. 6a

b *Liquid flow dynamics in nanotubes*

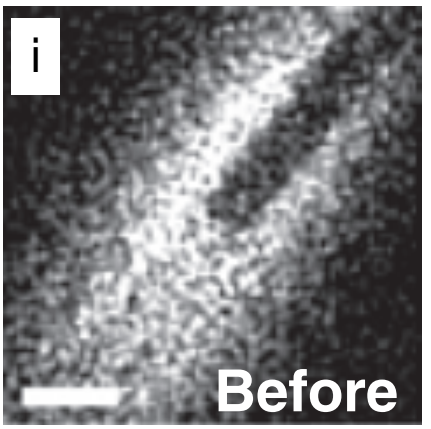

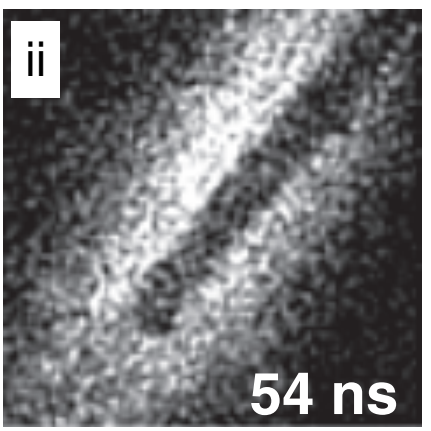

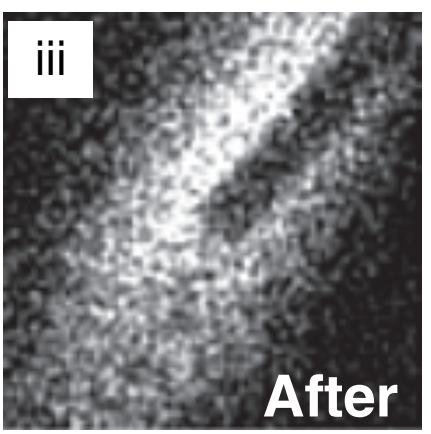

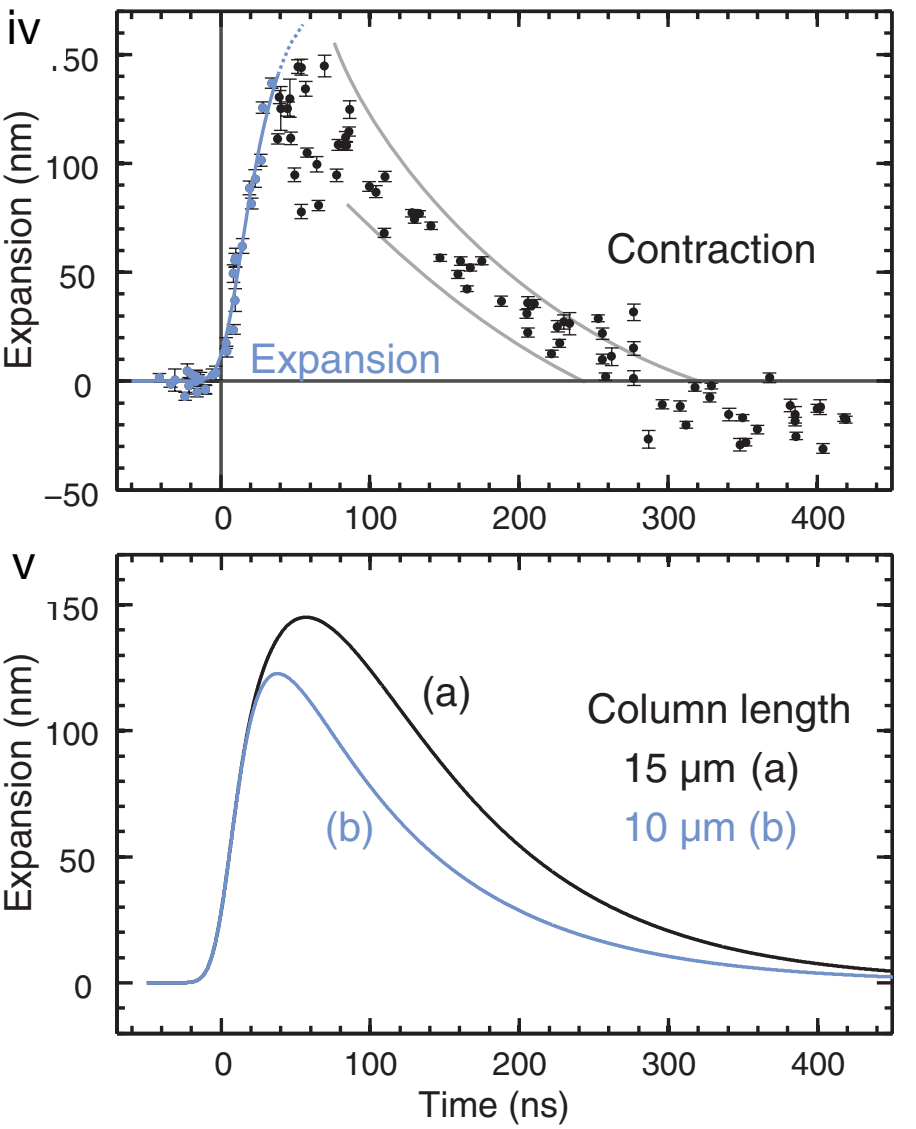

Fig. 6b

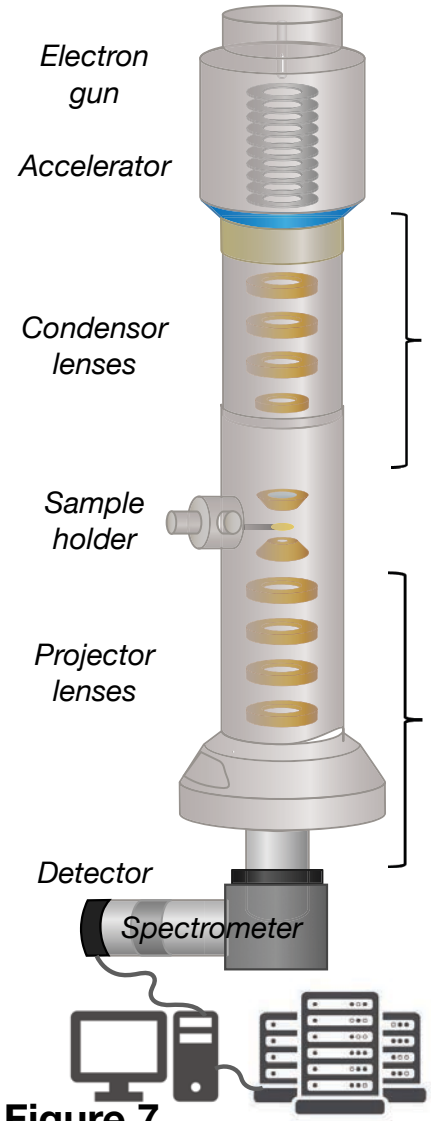

Goals	Enabling Technologies
• Generate high-brightness electron beams (continuous or pulsed) • Flexibility in gun configuration	• Thermionic and FEG guns • Photoelectron guns • Radio frequency (RF) guns • Ultracold gas sources
• Increase electron throughput	• Extra magnetic lenses
• Manipulate beam properties (coherence, energy spread, time duration, time structure)	• Beam deflectors and RF cavities • Monochromators • Apertures
• New ways to trigger sample • Combine stimuli • Increase sample stability • Increase spatial and temporal resolution	• Wide-gap objective lens • Aberration correction • Custom sample holders • Complex sample environments • Drift correction schemes
• Manipulate beam properties	• Beam deflectors and RF cavities • Apertures/phase plates
• Increase camera resolutions and quantum efficiency	• New pixel technologies • Fast electronics • Synchronization schemes
• Faster data storage • On-the-fly analysis	• Artificial intelligence, machine learning, compressed sensing • Supercomputing facilities

Chemical Dynamics

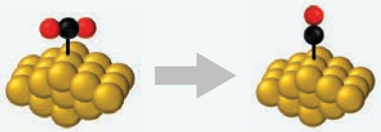

Image catalytic reactions taking place on particle surfaces

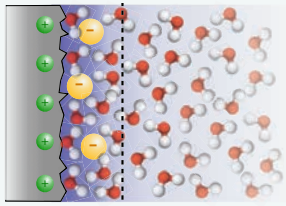

Determine the evolving atomic-scale structure of solid-liquid interfaces in electrochemical devices

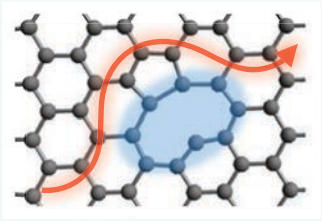

Observe energy transport across materials' interfaces and defects

Figure 7

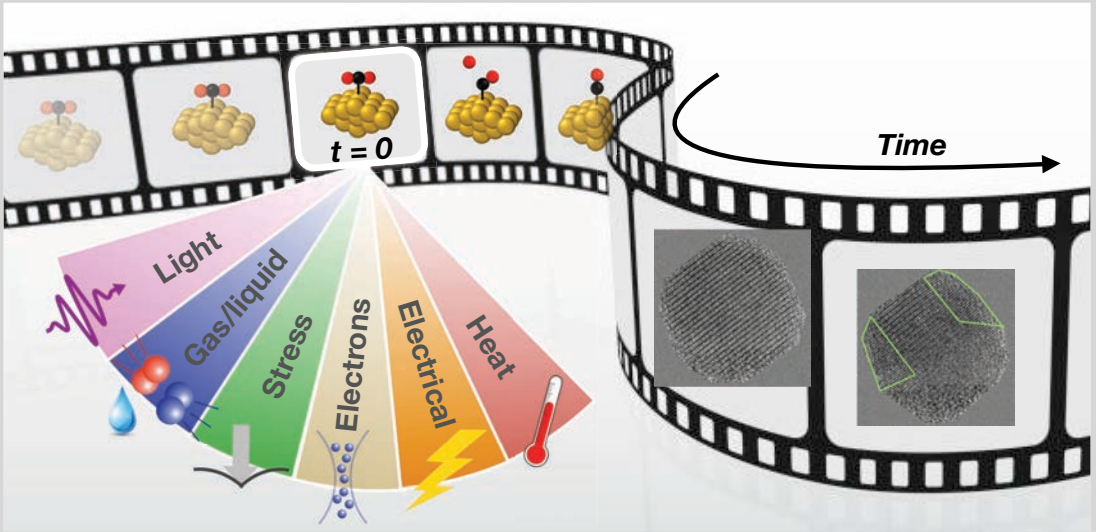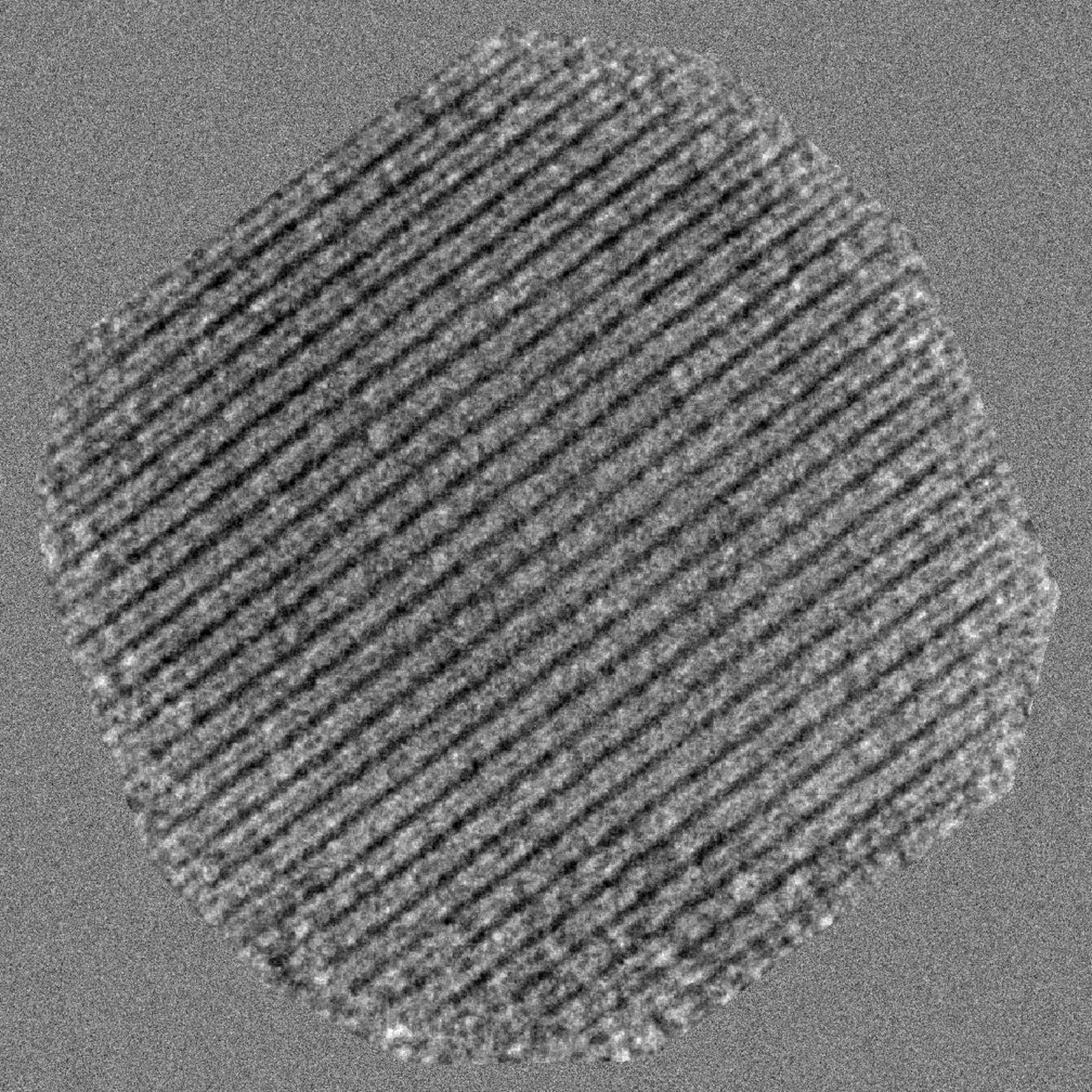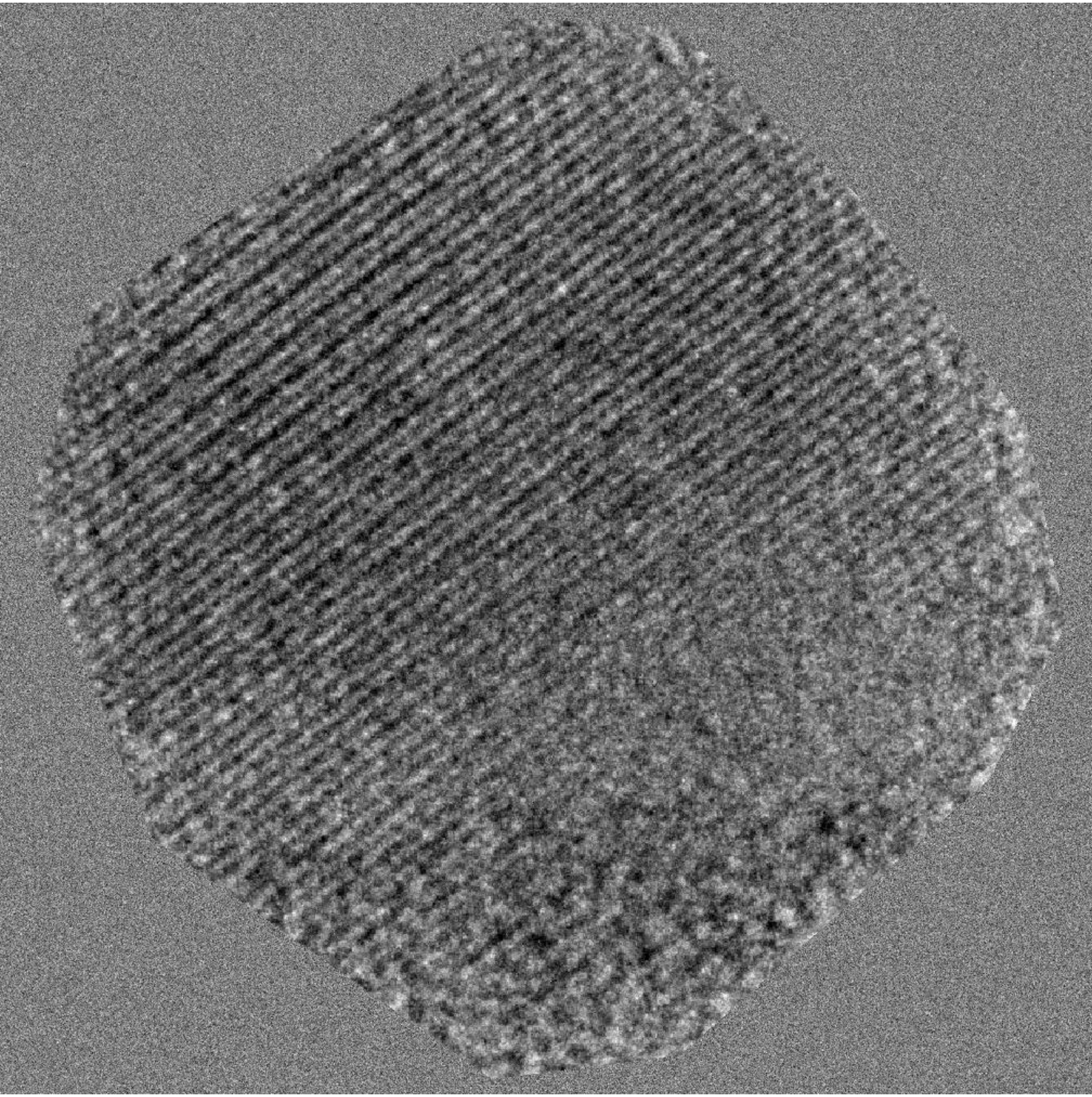
t = 0
Time
Light
Gas/liquid
Stress
Electrons
Electrical
Heat